European Journal of Medicinal Chemistry 298 (2025) 117990

Contents lists available at ScienceDirect

European Journal of Medicinal Chemistry

journal homepage: www.elsevier.com/locate/ejmech

Research paper

Design, synthesis, and biological evaluation of chalcone derivatives as selective Monoamine Oxidase-B inhibitors with potential neuroprotective effects

Giorgio Facchetti [a,1], Sara Marchese [b,1], Valentina Coccè [c], Luisa Doneda [c], Giulio Alessandri [c], Francesca Paino [c], Augusto Pessina [c], Luca Pinzi [d], Giulio Rastelli [d], Claudia Binda [b,*], Michael S. Christodoulou [e,**], Isabella Rimoldi [a]

[a] CRC StaMeTec, Department of Pharmaceutical Science, University of Milan, Via Golgi 19, 20133, Milan, Italy
[b] Department of Biology and Biotechnology Lazzaro Spallanzani, University of Pavia, Via Adolfo Ferrata 9, 27100, Pavia, Italy
[c] CRC StaMeTec, Department of Biomedical, Surgical and Dental Sciences, University of Milan, Via Pascal 36, 20133, Milan, Italy
[d] Department of Life Sciences, University of Modena and Reggio Emilia, Via Giuseppe Campi, 103, Modena, Italy
[e] Department of Food, Environmental and Nutritional Sciences, University of Milan, Via Celoria 2, 20133 Milano, Italy

ARTICLE INFO

Keywords:
Chalcones
Neuroprotective drugs
Human monoamine oxidase
Crystal structure
Inhibitor
SH-SY5Y neuroblastoma cell line

ABSTRACT

A series of chalcone derivatives was synthesized via Claisen–Schmidt condensation and further modified through selective reductions and amide couplings to explore their potential as monoamine oxidase B (MAO-B) inhibitors. Screening against recombinant human MAO-B identified compounds **4a**, **4b**, **4e**, and **5a** as potent inhibitors, showing submicromolar inhibition constants (K_i). Structure–activity relationship (SAR) analysis emphasized the relevance of a planar α,β-unsaturated carbonyl and specific aromatic substitutions for activity. Crystallographic studies showed conserved binding modes in the MAO-B active site, while computational analyses confirmed favourable interactions and conformational flexibility of compound **5a**. Cytotoxicity assays in normal and cancer cell lines indicated minimal toxicity for **5a**. Notably, **5a** also exhibited neuroprotective effects in SH-SY5Y cells exposed to 6-hydroxydopamine (6-OHDA), a model of Parkinson's disease. These findings demonstrated the importance of structural fine-tuning within the chalcone scaffold to achieve MAO-B selectivity and identify compound **5a** as a promising, non-toxic candidate for neurodegenerative disease treatment.

1. Introduction

Chalcones are naturally-occurring compounds, widely used in traditional medicine, with plant extracts to be the most important sources of these molecules [1]. Their structure, a three-carbon *α,β*-unsaturated carbonyl moiety joining two aromatic rings, occurs in a variety of biologically active natural and synthetic compounds and is considered as an open chain intermediate in the synthesis of flavones [2]. Chalcone and synthetic chalcone derivatives have shown important biological activities in medicinal chemistry and drug discovery [3,4], possessing a wide range of biological properties such as anti-viral [5], anti-oxidant [6], anti-fungal [7], anti-inflammatory [8], anti-microbial [9], and anticancer activities [10–15].

Over the past few years, chalcones have been considered promising structures for targeting neurodegenerative diseases by inhibiting the human monoamine oxidases A and B (hereafter referred as MAO-A and MAO-B) [16–20]. MAOs are a family of flavin adenine dinucleotide (FAD)-dependent enzymes, bound to the outer mitochondrial membrane, which catalyze the oxidative degradation of a number of neurologically important amine substrates including dopamine, norepinephrine, epinephrine, serotonin, and phenethylamine [21]. MAO consists of two isoforms, MAO-A and MAO-B, with a sequence similarity of ~73 % [22], but with distinct substrate and inhibition properties that depend also on their expression patterns in different tissues. Selective MAO-A inhibitors are specific for depressive disorders, whereas MAO-B selective inhibitors are used for treatments of

* Corresponding author.
** Corresponding author.
E-mail addresses: claudia.binda@unipv.it (C. Binda), michail.christodoulou@unimi.it (M.S. Christodoulou).
[1] These authors equally contributed to the manuscript.

https://doi.org/10.1016/j.ejmech.2025.117990
Received 23 June 2025; Received in revised form 15 July 2025; Accepted 18 July 2025
Available online 22 July 2025

neurodegenerative disorders, such as Parkinson's and Alzheimer's diseases [23,24].

In a previous study [25], we have identified a chalcone derivative (**1**, Fig. 1) as a selective MAO-B inhibitor exhibiting a potency comparable to the clinically used safinamide [26]. Interestingly, the lead compound **1** was elucidated to be positioned within MAO-B active site, with the trifluoromethyl (CF_3) substituent at the *meta* position situated at the entrance cavity underneath the protein surface [25], similarly to the favourable placement of the fluorine atom of safinamide in this conducive position [27]. Hence, based on the structure of the lead compound **1**, we have designed and synthesized a variety of analogues to identify novel selective inhibitors against MAO-B. Structure optimization and structure-activity relationship (SAR) analyses were centered on three specific regions (Fig. 1): the *m*-CF_3-benzene ring modified by the introduction of electron-withdrawing substituents (**Region A**), the intermediate α,β-unsaturated carbonyl moiety (**Region B**) and the benzene ring which is presumed to bind in front of the flavin cofactor (**Region C**) rationally redesigned by the introduction of substituents or different heterocycle rings. Collectively, these modifications were strategically planned to enhance the binding affinity to the active site of MAO-B. In relation to this, all compounds were evaluated for their efficacy against recombinantly expressed MAO-A and MAO-B using optimized enzymatic assays. Positive hits were further characterized through crystallographic studies to elucidate their binding mode within the MAO-B active site. Moreover, *in silico* structure-based studies including molecular docking to MAO-B active site were performed to aid in the definition of SAR properties. Finally, to complement the results on the purified proteins, cellular assays were conducted in first instance to assess possible cytotoxicity, and subsequently to determine their potential neuroprotective activity on human neuroblastoma-derived SH-SY5Y cells treated with 6-hydroxydopamine (6-OHDA) as a well-established cell-based model for Parkinson's disease (PD) [28].

2. Results and discussion

2.1. Chemistry

The small collection of chalcone derivatives was synthesized using the Claisen–Schmidt condensation methodology. Briefly, an aqueous solution of sodium hydroxide was added slowly to a methanol solution of the appropriate acetophenone (**2**). After the solution was cooled to room temperature, the appropriate benzaldehyde (**3**) was added, and the mixture was stirred overnight at room temperature to provide the corresponding chalcones (**4**) with moderate to excellent yields (Scheme 1) [25,29].

Ketone **5a** was obtained after selective reduction of the double bond of compound **1** in the presence of triethylsilane and TFA in DCM in very good yield, whereas alcohol **5b** was isolated after selective reduction of the carbonyl moiety of compound **1**, using $CeCl_3{\cdot}7H_2O$ and $NaBH_4$ in MeOH in excellent yield (Scheme 2) [30–32]. Total reduction of compound **1** with $NaBH_4$ gave alcohol **5c** in excellent yield (Scheme 2) [32]. Amides **9** and **10** were prepared from the condensation of 3-(trifluoromethyl)benzoic acid (**6**) and 3-(trifluoromethyl)phenylacetic acid (**7**) with benzylamine (**8**), respectively, using HATU as the coupling agent, in THF and DIPEA in very good yields (Scheme 3). All compounds were obtained in a range of 25–95 % yield and with >95 % purity, as determined by HPLC (Figs. S1–12, SI).

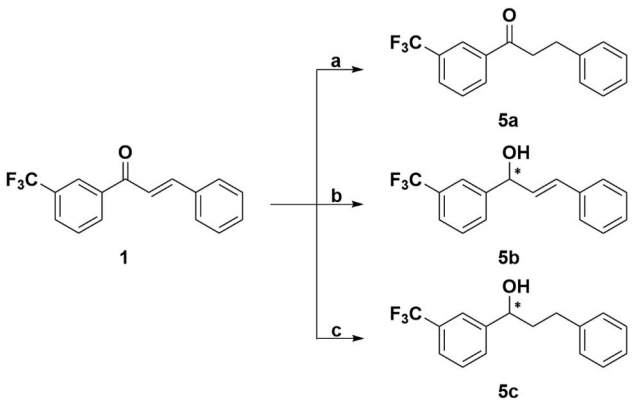

Scheme 2. Synthesis of compounds 5a–5c. Reagents and conditions: (a) Et_3SiH, TFA, DCM, rt, overnight, 75 % yield; (b) $CeCl_3{\cdot}7H_2O$, $NaBH_4$, MeOH, 3 h, rt, 95 % yield; (c) $NaBH_4$, MeOH, 1 h, rt, 95 % yield.

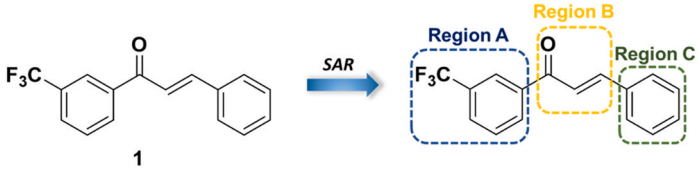

Fig. 1. Overall scheme showing the three regions selected for compound 1 optimization.

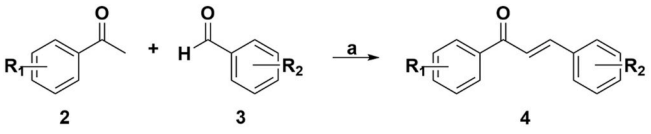

4a: R_1 = *m*-CF_3, R_2 = *p*-NO_2
4b: R_1 = *m*-CF_3, R_2 = *m*-NO_2
4c: R_1 = 2-Cl-5-CF_3, R_2 = H
4d: R_1 = 3,5-bis(CF_3), R_2 = H
4e: R_1 = *m*-CF_3, R_2 = *m,p*-(OCH_2O)-
4f: R_1 = *m*-CF_3, R_2 = 1*H*-imidazol-4-yl
4g: R_1 = *m*-CF_3, R_2 = 1*H*-imidazol-2-yl

Scheme 1. Synthesis of chalcone derivatives 4a – 4g. Reagents and conditions: (a) NaOH (30 % w/v), MeOH, rt, overnight, 25–95 % yield.

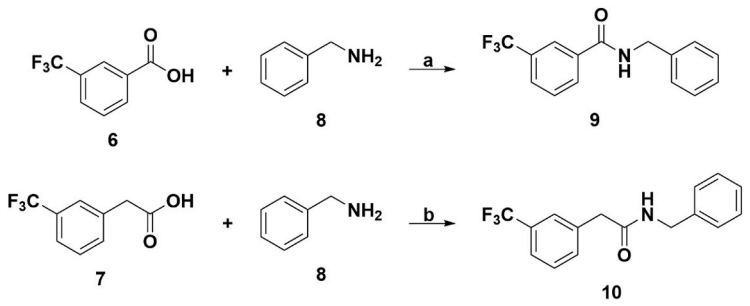

Scheme 3. Synthesis of compounds 9 and **10**. Reagents and conditions: (a) HATU, DIPEA, THF, 3 h, rt, 95 % yield; (b) HATU, DIPEA, THF, 3 h, rt, 75 % yield.

2.2. Biochemical and structural analysis of the inhibitors' binding mode to human MAO-B

All the synthetized chalcones derivatives were investigated for their inhibitory activity against the human recombinant MAO-B. In detail, we conducted a primary screening of compounds at 20 μM using the well-consolidated horse radish peroxidase (HRP)-coupled spectrophotometric assay by monitoring hydrogen peroxide as a secondary product of the MAO reaction. Safinamide was included as reference MAO-B selective inhibitor. The results highlighted the most effective strategy for chalcone scaffold optimization. Firstly, the introduction of an electron withdrawing substituent on the trifluoromethylbenzene moiety (Fig. 1, Region A), such as the addition of a chlorine atom at position 2 or of another trifluoromethyl group at position 3, did not enhance activity against MAO-B (Table 1, **4c** and **4d,** respectively). In this context, the earlier reported distinctive spatial orientation of the trifluoromethylbenzene toward the entrance cavity of the active site [25] suggests that the presence of an additional substituent on the ring would likely hinder its molecular access, potentially reducing the compounds' affinity for the protein. Secondly, the modification of the intermediate α, β-unsaturated carbonyl moiety (Fig. 1, Region B) revealed that the maintenance of the carbonyl group of **1** is crucial, as it positions the ligand within the active site, through a hydrogen bond with Cys172. Hence, the introduction of a hydroxyl group (-OH) (as in **5b**, **5c**), resulted in a minimal or negligible effect on MAO-B, likely caused by a structural clash with the same cysteine (Table 1). Interestingly, compounds preserving the carbonyl group alongside removal of the double bond appeared to be less potent in the initial screening, but this feature did not significantly compromise the inhibitory effects as demonstrated by **5a**. In contrast, the introduction of an amide group (compounds **9** and **10**) completely abolished the effect on MAO-B (Table 1). As expected, it is therefore essential that the ligand maintains both rigidities to accommodate within the MAO-B flat cavity and a certain degree of hydrophobicity [33].

Notably, the modifications that exhibited the most compelling profile were those made in **Region C** (Fig. 1). Firstly, the hydrophobic benzene ring, as for compound **1** [25], is crucial to maintain effective inhibition. Therefore, the substitution of the aromatic ring with an imidazole ring (Tables 1, **4f**, **4g**) led to a loss of activity against MAO-B. This aligns with the hydrophobic nature of the active site, which ensures aromatic substrate specificity [33]. As reported in Table 1, the introduction of specific substituents on the aromatic ring led to the major improvement in inhibitory effect. In particular, the most potent inhibitor (**4a**) yielded 90 % inhibition and it featured the insertion of a nitro group (-NO_2) at the *para* position. Interestingly, moving the –NO_2 group to the *meta* position on the benzene ring (**4b**) yet resulted in a potent inhibition (60 % activity). Lastly, the substitution of benzene with a benzodioxole ring (**4e**) also preserved strong activity, achieving 84.8 % inhibition. Remarkably, the most effective inhibitors **4a**, **4b**, **4e** and **5a** resulted to be highly selective for MAO-B, exhibiting minimal or no activity against human MAO-A (<10 % inhibition at 20 μM).

Chalcone derivatives inhibiting more than 50 % (**4a**, **4b**, **4e**, and **5a**) were thus selected for a complete characterization through inhibition constant (K_i) measurement (Table 1 and Fig. S13 and SI). Unsurprisingly **5a** exhibited the highest K_i (875 ± 160 nM), likely due to the single bond in **Region B** which increases its flexibility as mentioned above. By contrast, **4a**, **4b** and **4e** exhibited K_i in the very low submicromolar range (**4a** 245 ± 50 nM, **4b** 152 ± 20 nM, **4e** = 210 ± 40 nM, Table 1), and all were perfectly accommodated within the active site as confirmed by co-crystallization experiments where the electron density maps revealed unequivocal peaks corresponding to the ligands (Fig. 2a, b, c), as better described in the following sections. These values are comparable to that measured for compound **1** in the same assay conditions (K_i = 337 ± 40 nM). It is worth to specify that in our previous study [25] the lower K_i reported for **1** was due to the different experimental conditions (pre-incubation of the enzyme with the inhibitor, usage of microsomal human MAO-B rather than detergent-solubilized protein).

Crystallographic studies were performed to investigate the binding mode of **4a**, **4b**, **4e** and **5a** to human MAO-B active site by following well-established co-crystallization procedures [27]. The coordinates of MAO-B in complex with **1** (PDB code 7B0V [25]) deprived of the inhibitor atoms and of the water molecules were used as starting model to determine the structures of the enzyme bound to **4a**, **4b**, **4e** at 1.8, 1.6, 1.7 Å resolution, respectively (Fig. 2 and Table T1, SI). No significant differences between A and B chains (MAO-B dimer) of the asymmetric unit were observed, so we will henceforth refer to A for the description of the structures. Inspection of the structure of human MAO-B co-crystallized with **5a** (1.8 Å resolution) revealed residual electron density within the active site (data not shown) which could not be fitted with the inhibitor molecule. As observed in the past, this is probably due to low occupancy which may result from a high degree of flexibility of **Region B** lacking the double bond. Despite a similar inhibition potency with respect to the other chalcone derivatives, it is likely that **5a** features a more dynamic interaction with the active site which does not yield a stable enzyme-inhibitor complex required for crystallographic studies.

All the inhibitors showed a conserved binding mode with respect to **1**, with the trifluoromethyl-substituted ring (**Region A**) in *meta* position bound in the entrance cavity. The central linker moiety (**Region B**) adopts a planar conformation and the aromatic rings at the two ends are positioned nearly identically, with the inner one perpendicular to the flavin and the other slightly tilted (Figs. 2 and 3a). Presumably, unlike **5a**, the conjugated sp^2 double bond in the three new chalcone derivatives promotes planarity within the active site, in agreement with what has been observed in most of the previously published *non-covalent* MAO-B-inhibitor complexes [25,26,33,34]. Indeed, in all structures the amino acid residues adopt the same conformation within the active site, which results in an almost perfect superposition of the ligand cores (Fig. 3a, root-mean-square deviations for Cα atoms between 0.108 and 0.174 Å). This is particularly evidenced by the –NO_2 group of **4a** (Fig. 3a, depicted in sea green) that perfectly overlaps with the benzodioxole ring of **4e** (Fig. 3a, depicted in cornflower blue. The most pronounced difference appears when the –NO_2 substituent is in *meta* (**4b**), which points upwards to the residue Phe343 allowing the ligand to be closer to the flavin ring with respect to **4a** and **4e** (Fig. 3a). This small but significant

Table 1
Inhibition of human recombinant MAO-B by chalcones derivatives.

Compound	Structure	% Inhibition human MAO-B[a]	K_i (nM)[b,c]
1	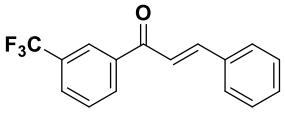	ND[d]	337 ± 40
4a	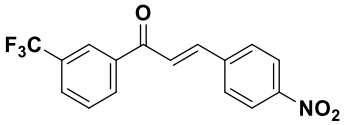	90.0	245 ± 50
4b	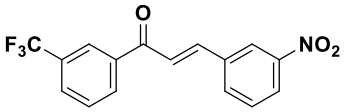	60.0	152 ± 20
4c	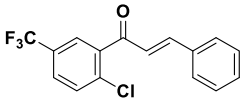	8.7	ND[d]
4d	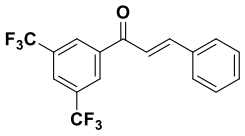	13.0	ND[d]
4e	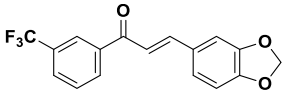	84.8	210 ± 40
4f	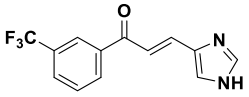	25.6	ND[d]
4g	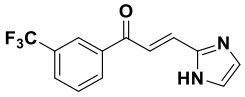	19.1	ND[d]
5a	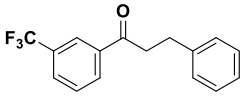	56.5	875 ± 160
5b	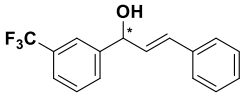	41.3	ND[d]
5c	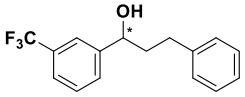	0.0	ND[d]
9	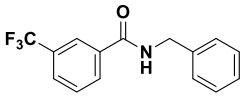	14.9	ND[d]
10	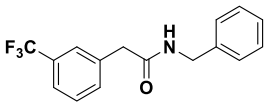	8.5	ND[d]
Safinamide	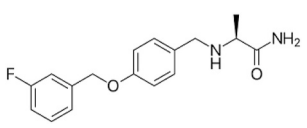	90.1	634 ± 14

[a] Compounds tested at 20 μM.

[b] Inhibition constant values were determined for compounds inhibiting MAO-B > 50 % at 20 μM.
[c] Values are reported as mean ± SE (standard error) of two biologically independent experiments.
[d] ND: not determined.

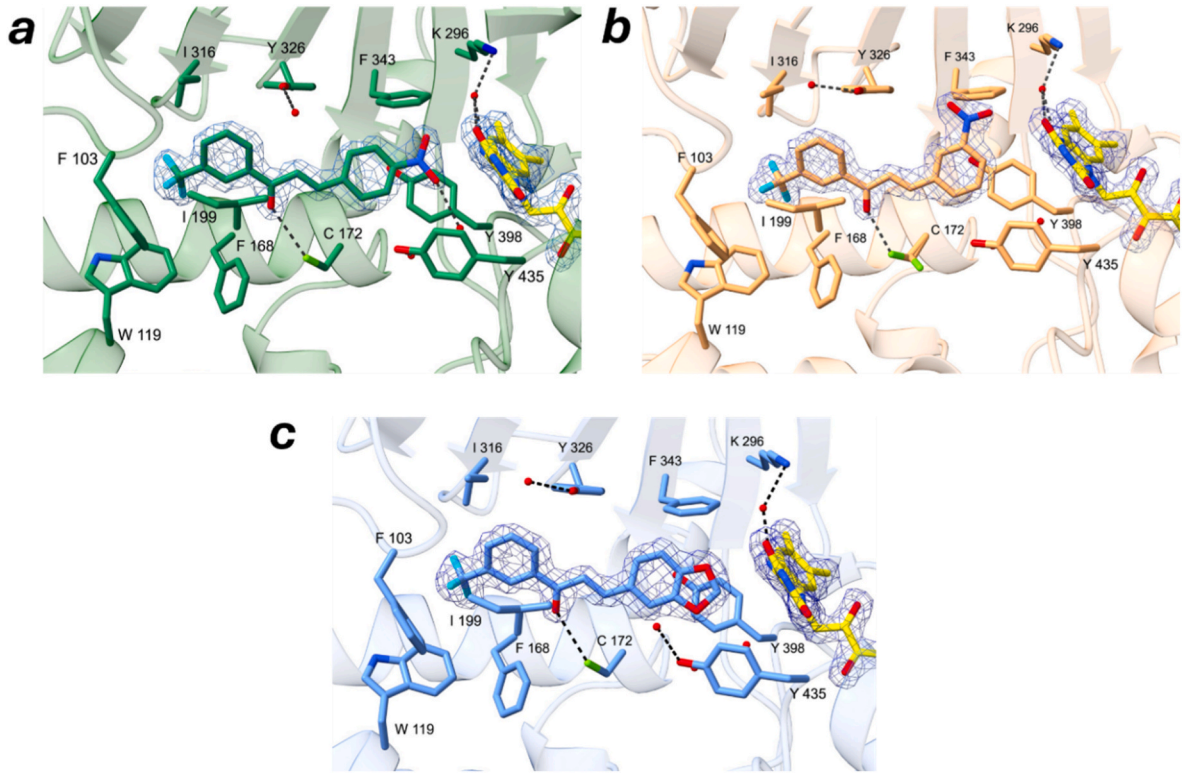

Fig. 2. Crystal structures of human MAO-B in complex with (a) 4a, (b) 4b, (c) 4e. In all the structures, the active site and bound inhibitor adopt the same conformation in both monomers of the dimer (chains A and B) within the asymmetric unit. For clarity, only chain A is shown. The FAD cofactor is depicted in stick representation, with carbon atoms in yellow, nitrogen in blue and oxygen in red. The refined $2F_o - F_c$ electron density map for the inhibitor molecule (contoured at 1.5σ) is shown in blue chicken-wire style. The residues surrounding the cavity are represented as sticks with nitrogen, oxygen, and sulfur atoms in blue, red, and green, respectively. Carbon atoms of both MAO-B residues and inhibitors are in sea green (**4a**), sandy brown (**4b**) and cornflower blue (**4e**). The fluorine atoms of the inhibitors are in light blue. Water molecules are depicted as red spheres and hydrogen bonds as dashed lines. Residue Gln206 was removed for the sake of clarity of the figure. (For interpretation of the references to color in this figure legend, the reader is referred to the Web version of this article.)

shift in **4b** binding leads to a shorter hydrogen bond with Cys172 with respect to **4a** and **4e** (Fig. 2a, b, c) and a double conformation of this residue observed also in other crystal structures [28], which results from a partial clash of the –SH group with the inhibitor carbonyl oxygen and compensates for suboptimal SH···O H-bond length at shorter distances. This scenario was found also in the structure in complex with **1** [25] whose positioning within the active site aligns well with that of **4b** (Fig. 3b). Interestingly, the two ligands are perfectly superimposable with a minor shift of the aromatic ring towards the flavin due to the *meta*-substituted $–NO_2$ group, which induces a small downward

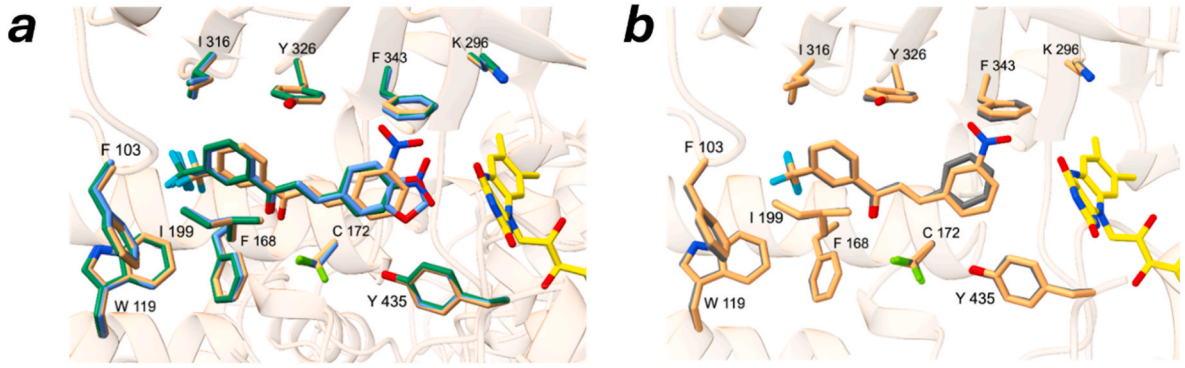

Fig. 3. Superposition of MAO-B structures in complex with (a) 4a, 4b and 4e; (b) 4b and compound 1. (a) The colors are consistent with those used in Fig. 2. **(b) 4b** is represented as in Fig. 2, compound **1** is represented with carbon atoms in grey (PDB code 7B0V). In both structures Cys172 is in a dual conformation. The root-mean-square deviation (RMSD) for Cα atoms is 0.111 Å. For the sake of clarity, to better appreciate the differences among the ligand binding modes, residue Tyr398, water molecules and hydrogen bonds shown in Fig. 2 have been omitted. (For interpretation of the references to color in this figure legend, the reader is referred to the Web version of this article.)

deviation. Collectively, these studies demonstrated that chalcone derivatives **4a**, **4b**, **4e** and **5a** are effective and promising human MAO-B inhibitors.

2.3. Molecular modelling studies on MAO-B

Docking calculations were performed into the 7B0V crystal structure [25] to aid in the discussion of SAR analysis. This structure was selected among the ones available as it is in complex with compound **1**, strictly related to the investigated series. Docking calculations were performed with the XP protocol available in Glide (Schrödinger 2025-1) [35,36], retaining three best scoring poses for each ligand; this allowed to further strengthen the reliability of the predicted poses. The ability of the docking protocol to retrieve the correct binding mode for (*E*)-3-phenyl-1-(3-(trifluoromethyl)phenyl)prop-2-en-1-one (SKB, compound **1**) co-crystallized compound was tested by performing redocking experiments, obtaining RMSD values between the docking and the crystallographic poses always within 1.5 Å, which is below the commonly accepted threshold of 2.0 Å. Docking experiments on the investigated series provided poses perfectly in agreement with those experimentally observed for **4a**, **4b**, and **4e** (Fig. 2 and Fig. S14 of the docking with **4a, 4b, 4e, SI).**

Interestingly, the poses predicted for compounds that showed inhibition below 15 % (**4c**, **4d**, **5c**, **9**, **10**, Fig. S15 and SI) showed orientations consistent with those of **4a**, **4b**, and **4e**, with the trifluoromethylphenyl ring (**Region A** in Fig. 1) that extends toward the entrance of the MAO-B cavity, while the other aromatic ring (**Region C** in Fig. 1) binding in proximity to FAD. Nevertheless, none of them was able to establish a H-bond interaction with the key residue Cys172 and steric clashes were observed with active site residues. In particular, **4c** presents a sterically hindered substitution with a chlorine atom in **Region A** (Fig. S15a and SI), which compromises the coplanarity of the phenyl with the rest of the molecule, and results in steric clashes with the side chain of Phe168. Similar considerations arise also for compound **4d**, whose additional trifluoromethyl moiety provides steric clashes with the side chain of Leu167 and Phe168, and Ile316 and Tyr326 (Fig. S15b and SI). Although compounds bearing an imidazole ring in **Region C** (*i.e.,* **4f** and **4g**) were not predicted to perform favourable H-bond interactions with the hot-spot residue Cys172 (Fig. 4a and b), they showed about 20 % inhibition. These compounds resulted to be shifted 0.8 Å (**4f**) and 0.7 Å (**4g**) towards the FAD cofactor with respect to the most potent compound of series **4b**, the imidazole moiety being placed near the conserved waters in search of H-bond interactions.

Interestingly, docking calculations for **5a** predicted two poses with

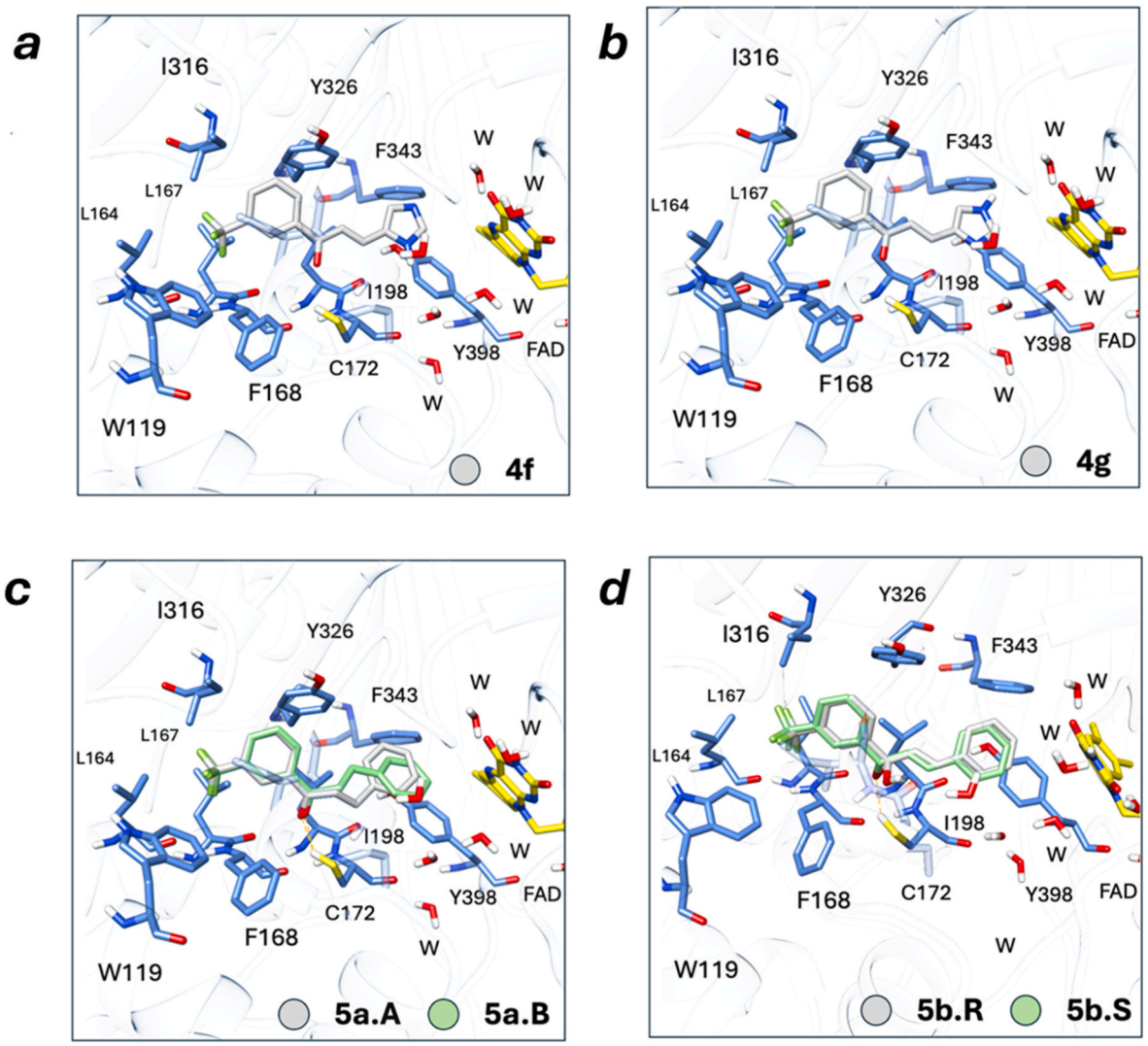

Fig. 4. Molecular modelling. Panels a, b, c and d report the predicted binding mode of **4f**, **4g**, **5a**, and **5b**, respectively, into the MAO-B active site. Ligands and key binding site residues are reported as sticks. Carbon atoms of both MAO-B residues and inhibitors are in light grey and cornflower blue, respectively. (For interpretation of the references to color in this figure legend, the reader is referred to the Web version of this article.)

almost identical scores (*i.e.* −11.9 kcal/mol and −11.8 kcal/mol for poses A and B, respectively; Fig. 4c) showing slightly different arrangements of the ethyl linker in **Region B** of the scaffold, in both of which the carbonyl establishes a H-bond with Cys172. Similar results were also observed after rescoring by means of the Prime MM-GBSA utility (Schrödinger 2025-1), although in this case the MM-GBSA scores were slightly in favour of pose A (MM-GBSA score of −72.5 kcal/mol and −70.8 kcal/mol for poses A and B, respectively). Such variability is in line with the higher conformational flexibility of compound **5a**, as already evidenced by the crystallographic study, which may be attributed to the lack of the double bond in the linker region. In the case of **5b** two highly overlapping poses were predicted for the *R* and *S* enantiomers (Fig. 4d). In the *R*-enantiomer the hydroxyl group interacts with the backbone of Ile198, whereas in the *S*-enantiomer it establishes a H-bond interaction with the key residue Cys172, although the longer C—OH bond (with respect to C═O) may not be favourable for an interaction with the SH group of Cys172.

In the more flexible derivate **5c**, two significantly different poses were observed (Fig. S15c and SI) and in both of them the ligand was not able to interact with Cys172. Finally, the introduction of an amide moiety in the scaffold (*e.g.* **9** and **10**, Fig S15d and S15e, SI) resulted in the loss of the H-bond interaction of the compounds with the hot-spot residue Cys172 into the MAO-B binding site, thus resulting in lack of significant activity towards this target.

2.4. In silico drug-likeness evaluation of the chalcone derivatives

Blood-Brain-Barrier (BBB) permeability is one of the key factors to be considered when developing drug candidates acting on central nervous system. In this regard, the chalcone structure represents a promising scaffold for the development of potential CNS therapeutic agents, given its low molecular weight and the potential easily optimizable lipophilicity profile. Previous studies on chalcone molecules investigated as CNS-targeted agents showed favourable BBB penetration [37,38] in PAMPA assays, which are employed to forecast BBB passive passage of drugs. To evaluate whether the compounds developed in this study might cross the BBB and feature promising properties as CNS therapeutic agents, *in silico* predictions of key molecular descriptors were carried out with QikProp (Schrödinger 2025-1) [39]. QikProp allowed the prediction of key molecular properties associated only to passive BBB permeability. Besides, the topological polar surface area (TPSA) molecular descriptor, which is commonly employed to predict the ability of molecules to cross biological membranes, was also evaluated for the compounds by using a tailored python script implemented with the RDKit library (https://www.rdkit.org/).

Results of the analyses showed that all compounds present desirable properties as CNS therapeutic agents, and in agreement with the commonly accepted Ghose's rules for BBB passage [40]. In particular, all derivatives present favourable values of predicted brain/blood partition coefficient (logBB), solvent accessible surface area (SASA), as predicted by QikProp (Table 2). Similar considerations can be drawn for the predicted apparent MDCK cell permeability (*i.e.,* QPPMDCK in Table 2), which is considered to be a good surrogate of the blood-brain barrier, and the molecular flexibility (#rotor in Table 2). In addition, all compounds met the range of values proposed for TPSA by Ghose A. et al. [40] for optimal BBB permeability. Overall, the CNS parameter resulted to be favourable for all chalcone derivates, except for **4f** and **4g** (Table 2).

Additional evaluations were also carried out on selected ADME (absorption/distribution/metabolism/excretion) properties of the compounds, including solubility (QplogS), volume, globularity (glob), logP (QPlogPo/w), Caco2 cell permeability (QPPCaco), number of hydrogen bonds donors (NumHBD) and acceptors (NumHBA), and the predicted binding to human serum albumin (QPlogKhsa), which are often investigated in preclinical settings. Of note, for all the compounds each parameter falls within the optimal range except for compound **4d**, which showed solubility properties (QPlogS) slightly outside the recommended values.

2.5. Cell-based assays: antiproliferative analysis, cell viability and preliminary evaluation of the neuroprotective effect on the SH-SY5Y neurodegeneration model

The antiproliferative activity of the three most promising molecules, **4a**, **4e** and **5a,** was evaluated against two normal cell lines (adipose tissue derived mesenchymal stromal cells AT -MSCs, and human dermal fibroblasts hSDFs, Fig. 5) and three cancer cell lines (human melanoma A-375, human glioblastoma U87-MG, human neuroblastoma SH-SY5Y, Fig. 6). Compound **4b** was excluded as it represents an analogue of **4a** specifically designed later along these studies to probe the effect of the different position of the $–NO_2$ group on the interaction within the enzyme active site. Briefly, compounds **4a** and **4e** showed a clear dose-dependent antiproliferative activity toward both normal and cancer cells, with varying IC_{50} values reported in Fig. 5c and 6d. Remarkably, **5a** was the safest compound among those tested, showing no significant inhibitory effects on the proliferation of either normal or cancer cells and with a significant outcome on the neuroblastoma cells (SH-SY5Y), at concentrations up to the maximum tested dose of 40 μM.

Considering the results obtained on this cell line, namely, the limited effect of **5a** on the viability of SH-SY5Y neuroblastoma cells, we

Table 2
Selected BBB-related molecular descriptors of the compounds investigated in this study.

Compound	CNS	SASA	TPSA	QPPMDCK	QlogBB	Volume	#rotor
1	1	528.6	17.1	8921.3	0.2	877.7	4
4a	**−1**	567.3	60.2	897.9	−0.9	950.8	5
4b	**−1**	567.6	60.2	898.4	−0.9	951.3	5
4c	1	551.0	17.1	10000	0.4	920.7	4
4d	2	580.9	17.1	10000	0.5	976.0	4
4e	1	533.0	35.5	8925.5	0.2	913.9	4
4f	**0**	497.8	45.8	2371.2	−0.3	815.5	4
4g	**0**	500.4	45.8	2901.4	−0.3	818.1	4
5a	1	537.1	17.1	9699.1	0.2	896.9	4
5b	1	529.4	20.2	8763.1	0.2	888.8	4
5c	1	544.5	20.2	10000	0.2	912.2	5
9	1	528.1	29.1	9772.4	0.3	877.5	3
10	1	562.1	29.1	10000.0	0.3	939.9	4

Values outside recommended ranges of Ghose A. et al. [40] are highlighted in bold. Recommended value ranges according to the QikProp (Schrödinger 2025-1) manual are the following: **CNS** (predicted central nervous system activity): −2 (inactive) - +2 (active) (Ghose's recommended range: >0); **SASA** (total solvent accessible surface area): 300 Å – 1000 Å (Ghose's recommended range: 320 Å – 735 Å); **TPSA** (topological polar surface area): Ghose's < 76 $Å^2$; **QPPMDCK** (predicted apparent MDCK cell permeability in nm/sec.): <25 poor, >500 great; **QlogBB** (predicted brain/blood partition coefficient): −3.0 – 1.2; **Volume** (predicted total solvent-accessible volume in cubic angstroms): 500 $Å^3$ – 2000 $Å^3$ (Ghose's recommended range: 460 $Å^3$ – 1250 $Å^3$); **#rotor** (number of rotatable bonds): 0–15.

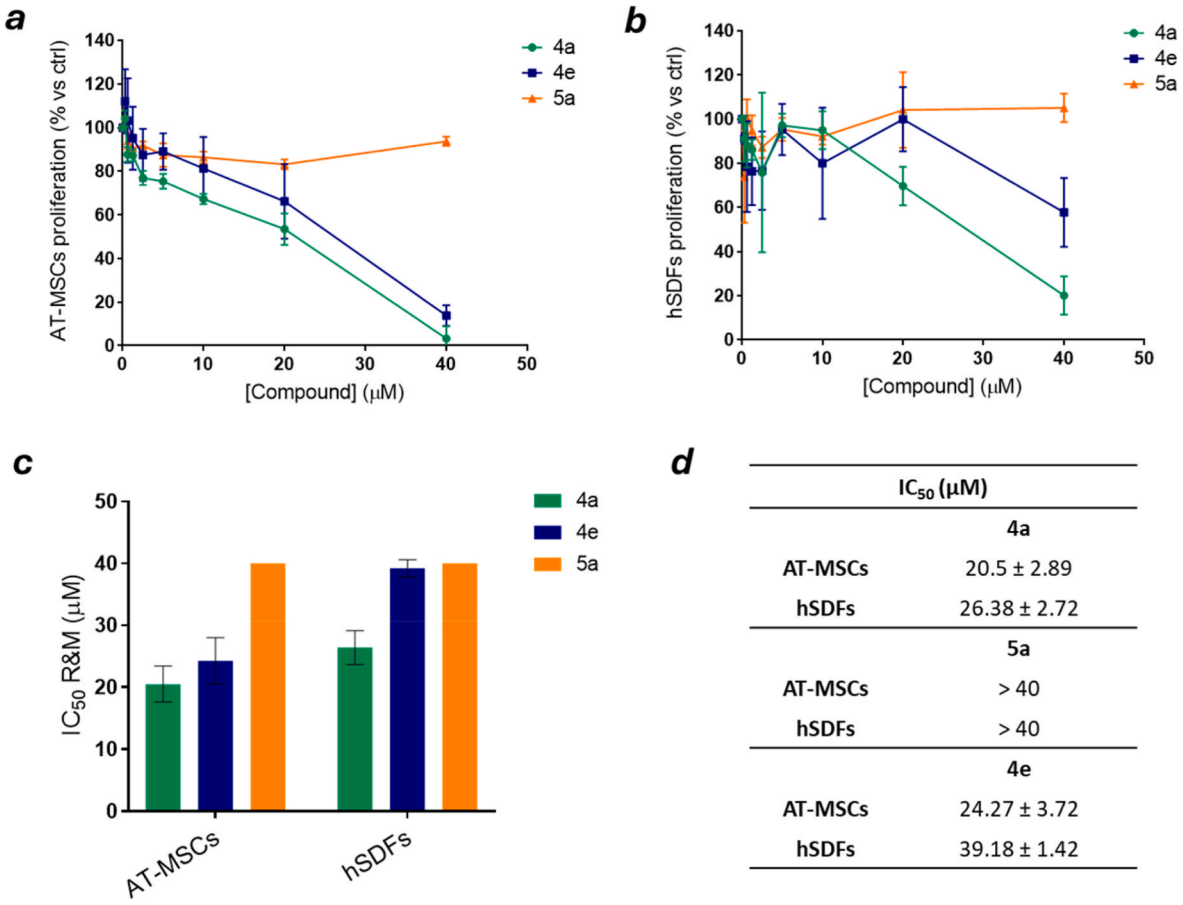

IC_{50} (μM)	
	4a
AT-MSCs	20.5 ± 2.89
hSDFs	26.38 ± 2.72
	5a
AT-MSCs	> 40
hSDFs	> 40
	4e
AT-MSCs	24.27 ± 3.72
hSDFs	39.18 ± 1.42

Fig. 5. ***In vitro*** **antiproliferation activity of 4a, 4e and 5a compounds on normal cells.** The effect of increasing concentrations of compounds **4a**, **4e** and **5a** was evaluated by a 7-day antiproliferation MTT assay on AT-MSCs cells, **(a)**; and on hSDFs cells **(b)**. The effect was expressed as a percentage of the optical density measured in cultures that did not receive compounds (100 % proliferation). The histogram **(c)** and the table **(d)** report the IC_{50} values expressed as mean ± standard deviation (SD) of three independent experiments with Reed & Muench (R&M) formula [63].

proceeded to evaluate its potential neuroprotective activity. SH-SY5Y cells treated with 6-hydroxydopamine (6-OHDA) are a widely used *in vitro* model for the study of neurodegenerative diseases such as PD[23], particularly for the evaluation of the effects of anti-MAO compounds developed as potential neuroprotective drugs. To determine the optimal experimental conditions for the following evaluation of the neuroprotective effects, we first assessed the cell viability in SH-SY5Y cells treated with varying concentrations of **5a** at 2 h, evidencing very low cytotoxicity at concentrations up to 100 μM (Fig. 7a). The cytotoxicity of 6-OHDA at the 24-h time point revealed a clear dose-response effect with an IC_{50} value of 140.5 ± 46.2 μM (Fig. 7b).

Based on these findings, we assessed the potential neuroprotective effect of compound **5a** by pre-treating SH-SY5Y cells for 2 h with **5a** at concentrations of 12.5 μM, 25 μM, 50 μM, and 100 μM, followed by exposure to increasing concentrations of 6-OHDA for 24 h. As shown in Fig. 8, pretreatment with **5a** resulted in higher cell viability compared to non-pretreated cells, suggesting a potential protective effect against 6-OHDA-induced toxicity. Statistical analysis revealed that a significant increase in the IC_{50} of 6-OHDA ($p < 0.01$) occurred only with **5a** concentrations of 12.5 μM and 25 μM. At 50 μM, no statistically significant change was observed, and pretreatment with 100 μM showed no effect on the IC_{50} value (Fig. 8). This indicates that the neuroprotective activity of **5a** was observed only at concentrations of 12.5 μM and 25 μM. The lack of efficacy at 50 μM and 100 μM is likely due to the onset of the cytotoxic effects observed, though at a limited extent, at high **5a** concentrations (Fig. 7a) which may be even worsened by the 6-OHDA treatment. Importantly, the neuroprotective activity of **5a** was not compared with the well-established MAO-B inhibitors such as safinamide or rasagiline, both of which exhibit potent activity at concentrations near 1 μM [41]. Although preliminary, these findings underscore the need for further investigation to evaluate the potential of compound **5a** as a candidate for antiparkinsonian drug development. This is particularly justified by its demonstrated ability to inhibit recombinant human MAO-B, as a well-established enzyme involved in dopamine catabolism in the brain. Given that MAO-B hyperactivation has been linked to dopaminergic neuron degeneration in PD, this mechanism of action warrants deeper exploration [25]. Future studies should focus on examining the effects of lower concentrations of compound **5a** administered over extended pretreatment periods in SH-SY5Y cells. Such investigations could provide more definitive evidence of its neuroprotective properties and contribute to understanding how **5a** may modulate cellular processes commonly implicated in PD, including oxidative stress, mitochondrial dysfunction, and neuroinflammation [42].

3. Conclusions

This study presents a comprehensive exploration of chalcone-based compounds as selective human MAO-B inhibitors, combining synthetic chemistry, biochemical assays, structural studies both crystallographic and computational, and the biological evaluation in neurodegenerative-like cell models. The SAR analysis demonstrated that the α, β-unsaturated carbonyl system peculiar to the chalcone scaffold is critical for proper ligand positioning within the MAO-B active site, primarily through interactions with Cys172. Overall, the presence of imidazole rings and amide modifications, as well as the steric hindrance in **Region**

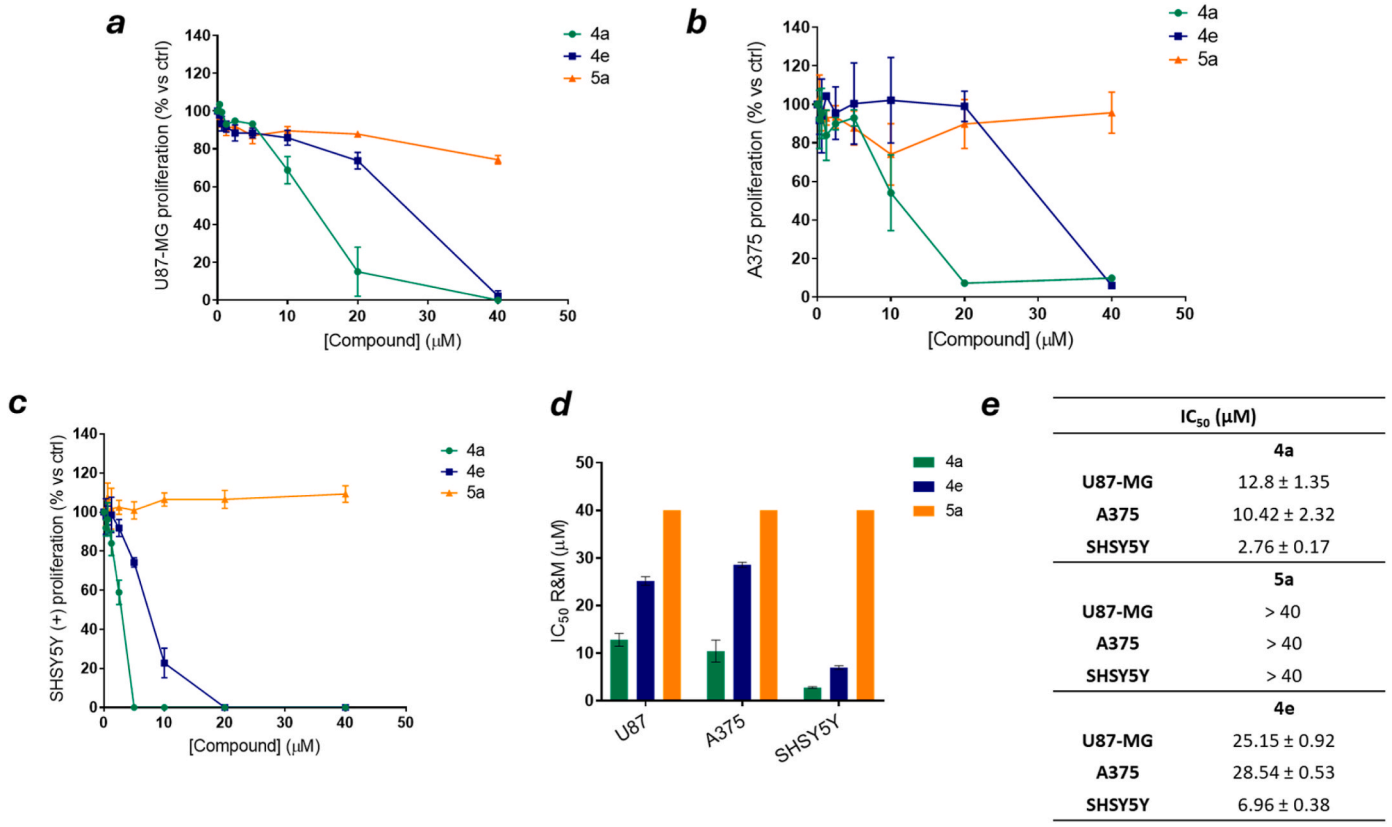

IC_{50} (μM)	
	4a
U87-MG	12.8 ± 1.35
A375	10.42 ± 2.32
SHSY5Y	2.76 ± 0.17
	5a
U87-MG	> 40
A375	> 40
SHSY5Y	> 40
	4e
U87-MG	25.15 ± 0.92
A375	28.54 ± 0.53
SHSY5Y	6.96 ± 0.38

Fig. 6. ***In vitro*** **antiproliferation activity of 4a, 4e and 5a compounds on tumoral cells.** The effect of increasing concentrations of compounds **4a**, **4e** and **5a** were evaluated by a 7-day antiproliferation MTT assay on human glioblastoma U87-MG (**a**), human melanoma A375 (**b**) and human neuroblastoma SH-SY5Y (**c**). The effect was expressed as a percentage of the optical density measured in cultures that did not receive compounds (100 % proliferation). The histograms (**d**) and the table (**e**) report the IC_{50} values expressed as mean ± standard deviation (SD) of three independent experiments with Reed & Muench (R&M) formula [63].

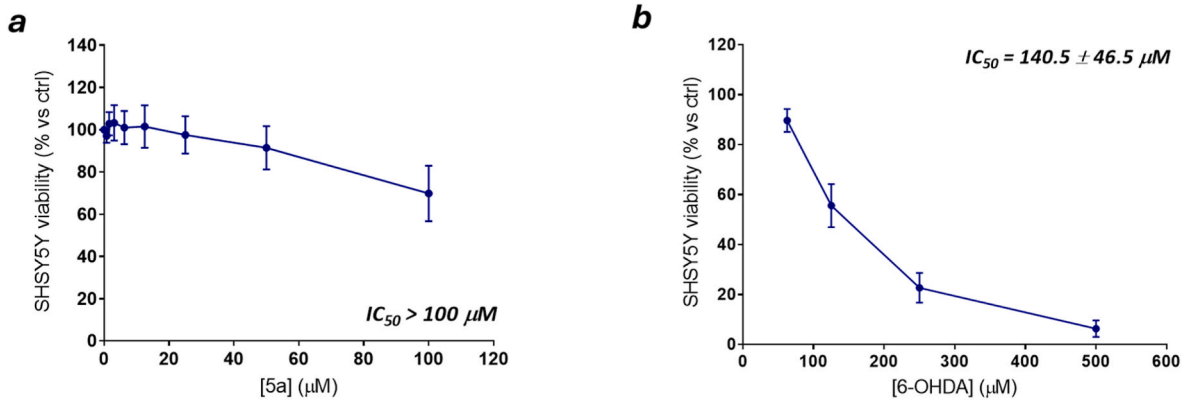

Fig. 7. ***In vitro*** **cytotoxicity of 5a and 6-OHDA on SH-SY5Y neuroblastoma cells.** The cytotoxic activity of **5a** compound was evaluated after 2 h (**a**) of treatment with different concentrations (from 0.78 to 100 μM) and expressed as cell viability (% of control cells). The cytotoxic activity of 6-OHDA was evaluated after 24 h (**b**) of treatment with different concentrations (from 62.5 to 500 μM) and expressed as cell viability (% of control cells). Values expressed as mean ± standard deviation (SD) of three independent experiments with Reed & Muench (R&M) formula [63].

A along with the lack of key H-bond interactions with Cys172 within MAO-B, have been identified as the major causes that impaired binding affinity. Aromatic substituents significantly modulate the inhibitory activity, with **4a**, **4b**, **4e** and **5a** emerging as the most promising derivatives. Structural investigations revealed a conserved binding mode with respect to **1**, confirming the requisite of planarity to improve their stable binding within the active site.

Importantly, **5a** derivative, even if slightly less potent, emerged for its target selectivity, together with the markedly low toxicity in cellular models and its promising neuroprotective potential. Although no stable enzyme-inhibitor complex suitable for crystallographic analysis was maintained due to its higher flexibility, docking studies using 7B0V structure in complex with compound **1** confirmed consistent binding poses for the compounds that resulted to be active on MAO-B in enzymatic assays and highlighted structural causes for the reduced MAO-B inhibition. *In vitro* cytotoxicity profiling against cancer and normal cell lines revealed a compound-specific activity, with **5a** showing negligible effects on cell viability. Most notably, **5a** exhibited promising neuroprotective effects in SH-SY5Y cells under oxidative stress induced by 6-OHDA, a validated PD cellular model. Pretreatment with **5a** at low

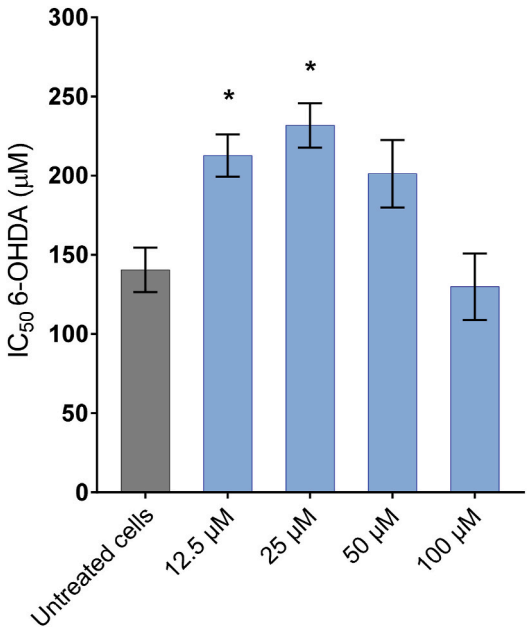

Fig. 8. Modulation of 6-OHDA cytotoxicity by 5a treatment on SH-SY5Y Neuroblastoma cells. The histogram reports the IC_{50} values expressed as mean ± standard error (SE) of 6-OHDA on untreated cells or on cells pretreated for 2 h with **5a** compound at four different dosages (12.5; 25; 50 and 100 μM). Values are expressed as mean ± standard deviation (SD) of three independent experiments. (*) $p = 0.01$.

micromolar concentrations (12.5 and 25 μM) significantly increased cell viability, suggesting its ability to mitigate neurotoxic damage induced by 6-OHDA. Although preliminary, these results highlight **5a** as a compelling lead compound for further neuropharmacological studies, considering its dual role, both as a selective MAO-B inhibitor and a neuroprotective agent, and standing out as a strong candidate for development as an antiparkinsonian drug. Further mechanistic investigations focusing on oxidative stress pathways, mitochondrial function, and neuroinflammation will be essential to confirm its therapeutic potential and elucidate its mode of action in neurodegenerative-relevant models.

4. Experimental section

Chemistry. Reagents and solvents were purchased from Sigma-Aldrich or Zentek and used without further purification. The NMR spectroscopic experiments were carried out on Bruker Avance I 400 MHz spectrometers (400, 101 and 282 MHz for ^{1}H, ^{13}C and ^{19}F respectively). All the experiments were recorded at 298 K using TMS as internal standard. HR-MS analyses were performed by using a QTof Synapt G2 Si spectrometer with an electrospray ionization source (Palmer, MA, USA). The MS spectra were obtained by direct infusion of a sample solution of 2 μg/mL in MeOH under ionization, ESI positive. FTIR spectra were collected by using a PerkinElmer (MA, USA) FTIR Spectrometer "Spectrum One" in a spectral region between 4000 and 450 cm^{-1} and analyzed by transmittance technique with 32 scansions and 4 cm^{-1} resolution. For chemical and biological structures, ChemDraw 23.1.2 and Biorender software were utilized.

4.1. Synthesis of α,β-unsaturated ketones

An aqueous solution of sodium hydroxide (30 % p/p, 10 mL) was slowly added to a methanol solution (12 mL) of the appropriate acetophenone (2.0 mmol). After the solution had been cooled to room temperature, the appropriate benzaldehyde (2.4 mmol) was added, and the solution was stirred overnight at the same temperature. Then, the precipitated solid was removed by filtration, washed with H_2O, and recrystallized from ethanol. If precipitation did not occur, the solvent was evaporated in vacuum, EtOAc was added, and the organic phase was washed with sat. NH_4Cl and brine, dried with Na_2SO_4, filtered, and evaporated. The desired product was obtained after purification by flash column chromatography.

(E)-3-(4-nitrophenyl)-1-(3-(trifluoromethyl)phenyl)prop-2-en-1-one (4a). According to the general procedure, the desired chalcone derivative **4a** was obtained from the reaction between 3′-(trifluoromethyl) acetophenone and 4-nitrobenzaldehyde after purification by flash column chromatography (silica gel, eluent mixture 8:2, *n*-Hex/EtOAc) and evaporation of the solvent, as a yellow amorphous solid (35 % yield). ^{1}H NMR (400 MHz, $CDCl_3$) δ = 8.33–8.23 (m, 4H, *p*-NO_2-Ph*H*), 7.91–7.82 (m, 4H, *m*-CF_3-Ph*H* and COCHC*H*), 7.73–7.63 (m, 2H, *m*-CF_3-Ph*H* and COC*H*CH) ppm. ^{13}C NMR (101 MHz, $CDCl_3$) δ = 188.25, 148.80, 142.71, 140.61, 138.09, 131.69, 131.50 (q, $J = 36.4$ Hz, *C*CF_3), 129.79–129.68 (m, Ar*C*(H)CCF_3), 129.54, 129.16, 127.43, 125.43–125.32 (m, Ar*C*(H)CCF_3), 124.77, 124.29, 123.93, 123.4 (q, $J = 271.9$ Hz, *C*F_3) ppm. ^{19}F NMR (282 MHz, $CDCl_3$) δ = −62.39 ppm. MS(ESI) for $C_{16}H_{10}F_3NO_3$: *m/z* [M]+ calcd 321.06; found 322.72 $[M+H]^+$. FT-IR (KBr) $\nu(cm^{-1})$ = 3112, 3080, 3043, 1737, 1663, 1606, 1594, 1534, 1345, 1202, 1167, 1121, 1070, 809, 690.

(E)-3-(3-nitrophenyl)-1-(3-(trifluoromethyl)phenyl)prop-2-en-1-one (4b). According to the general procedure, the desired chalcone derivative **4b** was obtained from the reaction between 3′-(trifluoromethyl) acetophenone and 3-nitrobenzaldehyde after purification by flash column chromatography (silica gel, eluent mixture 8:2, *n*-Hex/EtOAc) and evaporation of the solvent, as foam (70 % yield). ^{1}H NMR (400 MHz, $CDCl_3$) δ = 8.54–8.53 (m, 1H, *m*-NO_2-Ph*H*), 8.30–8.28 (m, 2H, *m*-NO_2-Ph*H* and *m*-CF_3-Ph*H*), 8.25–8.22 (d, 1H, $J = 8.4$ Hz, *m*-NO_2-Ph*H*), 7.97–7.94 (d, 1H, $J = 7.6$ Hz, *m*-CF_3-Ph*H*), 7.91–7.87 (m, 2H, *m*-CF_3-Ph*H* and COCHC*H*), 7.69–7.61 (m, 3H, *m*-NO_2-Ph*H*, *m*-CF_3-Ph*H* and COC*H*CH) ppm. ^{13}C NMR (101 MHz, $CDCl_3$) δ = 188.27, 148.29, 142.83, 139.92, 138.13, 136.27, 134.41, 131.66, 131.24 (q, $J = 36.0$ Hz, *C*CF_3), 130.14, 129.76–129.64 (m, Ar*C*(H)CCF_3), 129.64, 125.39–125.29 (m, Ar*C*(H)CCF_3), 124.86, 123.72, 122.56 (q, $J = 272.1$ Hz, *C*F_3) ppm. ^{19}F NMR (282 MHz, $CDCl_3$) δ = −62.69 ppm. MS(ESI) for $C_{16}H_{10}F_3NO_3$: *m/z* [M]+ calcd 321.06; found 322.25 $[M+H]^+$. FT-IR (KBr) $\nu(cm^{-1})$ = 3076, 2925, 2854, 1740, 1668, 1613, 1525,1323, 1269, 1202, 1166, 1117, 1071, 985, 921, 803, 693.

(E)-1-(2-chloro-5-(trifluoromethyl)phenyl)-3-phenylprop-2-en-1-one (4c). According to the general procedure, the desired chalcone derivative **4c** was obtained from the reaction between 2′-chloro-5′-(trifluoromethyl)acetophenone and benzaldehyde after purification by flash column chromatography (silica gel, eluent mixture 95:5, *n*-Hex/EtOAc) and evaporation of the solvent, as yellow oil (42 % yield). ^{1}H NMR (400 MHz, $CDCl_3$) δ = 7.77–7.76 (m, 1H, 2-Cl-5-CF_3-Ph*H*), 7.72–7.69 (m, 1H, 2-Cl-5-CF_3-Ph*H*), 7.63–7.59 (m, 3H, 2-Cl-5-CF_3-Ph*H* and Ph*H*), 7.49 (d, 1H, $J = 15.8$ Hz, COCHC*H*), 7.46–7.44 (m, 3H, Ph*H*), 7.16 (d, 1H, $J = 15.0$ Hz, COC*H*CH) ppm. ^{13}C NMR (101 MHz, $CDCl_3$) δ = 192.26, 147.22, 139.77, 135.13, 134.11, 131.30, 130.98, 129.46 (q, $J = 37.0$ Hz, *C*CF_3), 129.11, 128.75, 128.07–127.97 (m, Ar*C*(H)CCF_3), 127.07, 126.46–126.34 (m, Ar*C*(H)CCF_3), 125.82,125.55, 123.36 (q, $J = 271.9$ Hz, *C*F_3) ppm. ^{19}F NMR (282 MHz, $CDCl_3$) δ = −62.30 ppm. MS (ESI) for $C_{16}H_{10}ClF_3O$: *m/z* [M]+ calcd 310.04; found 311.38 $[M+H]^+$. FT-IR (KBr) $\nu(cm^{-1})$ = 3016, 2970, 2948, 1741, 1575, 1436, 1367, 1228, 1217, 1123, 903, 769.

(E)-1-(3,5-bis(trifluoromethyl)phenyl)-3-phenylprop-2-en-1-one (4d). According to the general procedure, the desired chalcone derivative **4d** was obtained from the reaction between 3′,5′-bis(trifluoromethyl)acetophenone and benzaldehyde after purification by flash column chromatography (silica gel, eluent mixture 96:4, *n*-Hex/EtOAc) and evaporation of the solvent, as a pale-yellow solid (25 % yield). Data is consistent with the published literature [43]. ^{1}H NMR (300 MHz, $CDCl_3$): δ = 8.45 (br. s, 2H, 3, 5-bisCF_3-Ph*H*), 8.10 (s, 1H, 3, 5-bisCF_3-Ph*H*), 7.92 (d, 1H, $J = 15.6$ Hz, COCHC*H*), 7.71–7.68 (m, 2H,

Ph*H*), 7.51 (d, 1H, $J = 15.6$ Hz, COC*H*CH), 7.48–7.46 (m, 3H, Ph*H*) ppm. ^{13}C NMR (101 MHz, $CDCl_3$): δ = 187.32, 147.41, 139.87, 134.12, 132.29 (2C, q, $J = 34.0$ Hz, *C*CF_3), 131.33 (2C), 128.88, 126.26 (5C), 122.77 (2C, q, $J = 273.0$ Hz, *C*F_3), 120.21 ppm. ^{19}F NMR (282 MHz, $CDCl_3$) δ = −62.98 ppm. MS(ESI) for $C_{17}H_{10}F_6O$: *m/z* [M]+ calcd 344.06; found 345.28 $[M+H]^+$. FT-IR (KBr) $\nu(cm^{-1})$ = 3019, 2978, 2966, 2948, 1662, 1575, 1518, 1416, 1288, 957, 654.

(E)-3-(benzo[d] [1,3]dioxol-5-yl*)-1-(3-(trifluoromethyl)phenyl)prop-2-en-1-one (4e)*. According to the general procedure, the desired chalcone derivative **4e** was obtained from the reaction between 3′-(trifluoromethyl)acetophenone and piperonal after purification by flash column chromatography (silica gel, eluent mixture 9:1, *n*-Hex/EtOAc) and evaporation of the solvent, as yellow oil (95 % yield). ^{1}H NMR (400 MHz, $CDCl_3$) δ = 8.27 (s, 1H, *m*-CF_3-Ph*H*), 8.20 (d, 1H, $J = 4.6$ Hz, *m*-CF_3-Ph*H*), 7.85–7.83 (m, 1H, *m*-CF_3-Ph*H*), 7.81 (d, 1H, $J = 15.1$ Hz, COCH*CH*), 7.66 (t, 1H, $J = 7.8$ Hz, *m*-CF_3-Ph*H*), 7.36 (d, 1H, $J = 15.1$ Hz, COC*H*CH), 7.19 (s, 1H, Ph*H*), 7.16 (d, 1H, $J = 8.1$ Hz, Ph*H*), 6.87 (d, 1H, $J = 7.2$ Hz, Ph*H*), 6.05 (s, 2H, O*CH*$_2$O) ppm. ^{13}C NMR (101 MHz, $CDCl_3$) δ = 188.88, 150.32, 148.52, 145.92, 138.97, 131.69, 131.53, 131.20 (q, $J = 33.2$ Hz, *C*CF_3), 129.25, 129.08–129.00 (m, Ar*C*(H)CCF_3), 125.67, 125.27–125.19 (m, Ar*C*(H)CCF_3), 122.44 (q, $J = 271.5$ Hz, *C*F_3), 119.73, 108.75, 106.74, 101.76 ppm. ^{19}F NMR (282 MHz, $CDCl_3$) δ = −63.30 ppm. MS(ESI) for $C_{17}H_{11}F_3O_3$: *m/z* [M]+ calcd 320.07; found 321.67 $[M+H]^+$. FT-IR (KBr) $\nu(cm^{-1})$ = 3079, 3048, 2900, 1659, 1593, 1576, 1498, 1451, 1373, 1311, 1248, 1159, 1112, 1070, 1028, 933, 802, 687.

(E)-3-(1H-imidazole-4-yl*)-1-(3-(trifluoromethyl)phenyl)prop-2-en-1-one (4f)*. According to the general procedure, the desired chalcone derivative **4f** was obtained from the reaction between 3′-(trifluoromethyl) acetophenone and 4-imidazolecarboxaldehyde after purification by flash column chromatography (silica gel, eluent mixture 95:5, *n*-Hex/EtOAc) and evaporation of the solvent, as yellow oil (25 % yield). ^{1}H NMR (400 MHz, CD_3OD) δ = 8.31–8.28 (m, 2H, *m*-CF_3-Ph*H* and C*H*-imidazole), 7.92–7.90 (d, 1H, $J = 8.0$ Hz, *m*-CF_3-Ph*H*), 7.87 (d, 1H, $J = 15.2$ Hz, COCH*CH*), 7.78 (m, 1H, *m*-CF_3-Ph*H*), 7.76 (d, 1H, $J = 15.2$ Hz, COC*H*CH), 7.76–7.75 (m, 1H, *m*-CF_3-Ph*H*), 7.57 (s, 1H, C*H*-imidazole) ppm. ^{13}C NMR (101 MHz, CD_3OD) δ = 188.81, 138.87, 137.87, 137.59, 134.54, 131.51, 131.43, 129.48 (2C), 129.41, 128.85 (q, $J = 31.6$ Hz, *C*CF_3), 124.58 (q, $J = 272.8$ Hz, *C*F_3), 118.04 ppm. ^{19}F NMR (282 MHz, CD_3OD) δ = −64.15 ppm. MS(ESI) for $C_{13}H_9F_3N_2O$: *m/z* [M]+ calcd 266.07; found 267.79 $[M+H]^+$. FT-IR (KBr) $\nu(cm^{-1})$ = 3237, 2968, 2925, 1644, 1532, 1328, 1267, 1124, 1071, 977, 800, 692.

(E)-3-(1H-imidazole-2-yl*)-1-(3-(trifluoromethyl)phenyl)prop-2-en-1-one (4g)*. According to the general procedure, the desired chalcone derivative **4g** was obtained from the reaction between 3′-(trifluoromethyl) acetophenone and 2-imidazolecarboxaldehyde after precipitation of the product, filtration, and recrystallization from ethanol, as a yellow amorphous solid (55 % yield). ^{1}H NMR (400 MHz, CD_3OD) δ = 8.35–8.30 (m, 2H, *m*-CF_3-Ph*H*), 7.94 (d, 1H, $J = 7.9$ Hz, *m*-CF_3-Ph*H*), 7.91 (d, 1H, $J = 15.7$ Hz, COCH*CH*), 7.81–7.74 (m, 1H, *m*-CF_3-Ph*H*), 7.65 (d, 1H, $J = 15.6$ Hz, COC*H*CH), 7.30 (s, 2H, C*H*-imidazole) ppm. ^{13}C NMR (101 MHz, CD_3OD) δ = 188.05, 143.59, 138.34, 131.60, 131.26, 130.92 (q, $J = 33.2$ Hz, *C*CF_3), 129.61, 129.26–129.15 (m, Ar*C*(H)CCF_3), 125.28, 125.04, 124.69–124.65 (m, Ar*C*(H)CCF_3), 122.56 (q, $J = 271.5$ Hz, *C*F_3), 121.56 ppm. ^{19}F NMR (282 MHz, CD_3OD) δ = −64.45 ppm. MS (ESI) for $C_{13}H_9F_3N_2O$: *m/z* [M]+ calcd 266.07; found 267.30 $[M+H]^+$. FT-IR (KBr) $\nu(cm^{-1})$ = 3111, 3009, 2971, 2860, 1737, 1673, 1618, 1550, 1439, 1329, 1256, 1204, 1125, 1073, 974, 811, 741.

Synthesis of 3-phenyl-1-(3-(trifluoromethyl)phenyl)propan-1-one (5a). To a solution of compound (*E*)-3-phenyl-1-(3-(trifluoromethyl)phenyl) prop-2-en-1-one [25] (0.15 g, 0.54 mmol) in DCM (2.5 mL), triethylsilane (0.35 mL, 2.2 mmol) and TFA (0.17 mL, 2.2 mmol) were added and the new solution was stirred overnight at r.t. After the completion of the reaction, DCM was added, and the organic phase was washed with H_2O and brine, dried with Na_2SO_4, filtered, and evaporated. The desired product was obtained after purification by flash column chromatography (silica gel, eluent mixture 9:1, *n*-Hex/EtOAc) and evaporation of the solvent, as yellow oil (75 % yield). Data is consistent with the published literature [44]. ^{1}H NMR (400 MHz, $CDCl_3$): $\delta = 8.21$ (s, 1H, *m*-CF_3-Ph*H*), 8.15 (d, 1H, $J = 8.0$ Hz, *m*-CF_3-Ph*H*), 7.82 (d, 1H, $J = 8.0$ Hz, *m*-CF_3-Ph*H*), 7.60 (t, 1H, $J = 8.0$ Hz, *m*-CF_3-Ph*H*), 7.33–7.28 (m, 2H, Ph*H*), 7.27–7.18 (m, 3H, Ph*H*), 3.34 (t, 2H, $J = 7.6$ Hz, COC*H*$_2$CH$_2$), 3.10 (t, 2H, $J = 7.6$ Hz, COCH$_2$C*H*$_2$). ^{13}C NMR (101 MHz, $CDCl_3$) δ = 197.81, 140.89, 137.37, 131.62 (q, $J = 34.1$ Hz, *C*CF_3), 131.16, 129.54–129.32 (m, Ar*C*(H)CCF_3), 129.47, 128.63, 128.44, 127.76, 126.32, 125.05, 124.97–124.86 (m, Ar*C*(H)CCF_3), 123.62 (q, $J = 271.1$ Hz, *C*F_3), 40.59, 29.95 ppm. ^{19}F NMR (282 MHz, $CDCl_3$) δ = −63.04 ppm. MS(ESI) for $C_{16}H_{13}F_3O$: *m/z* [M]+ calcd 278.09; found 279.10 $[M+H]^+$. FT-IR (KBr) $\nu(cm^{-1})$ = 3016, 2970, 1744,1725, 1435, 1380, 1367, 1231, 1199, 1117, 900, 693.

Synthesis of (E)-3-phenyl-1-(3-(trifluoromethyl)phenyl)prop-2-en-1-ol (5b). To a solution of compound (*E*)-3-phenyl-1-(3-(trifluoromethyl) phenyl)prop-2-en-1-one [25] (0.15 g, 0.54 mmol) in MeOH (6.0 mL), $CeCl_3{\cdot}7H_2O$ (0.20 g, 0.54 mmol) was added and the new solution was stirred for 15 min at r.t. Then, $NaBH_4$ (0.020 g, 0.54 mmol) was added, and the new mixture was stirred for 3 h at r.t. After the completion of the reaction, the solvent was evaporated, EtOAc was added, and the organic phase was washed with H_2O and brine, dried with Na_2SO_4, filtered, and evaporated. The desired product was obtained after purification by flash column chromatography (silica gel, eluent mixture 9:1, *n*-Hex/EtOAc) and evaporation of the solvent, as oil (95 % yield). Data is consistent with the published literature [45]. ^{1}H NMR (400 MHz, $CDCl_3$): $\delta = 7.73$ (1H, s, *m*-CF_3-Ph*H*), 7.62 (1H, d, $J = 8.0$ Hz, *m*-CF_3-Ph*H*), 7.58 (1H, d, $J = 8.0$ Hz, *m*-CF_3-Ph*H*), 7.50 (t, 1H, $J = 8.0$ Hz, *m*-CF_3-Ph*H*), 7.42–7.38 (m, 2H, Ph*H*), 7.35–7.32 (m, 2H, Ph*H*), 7.29–7.26 (m, 1H, Ph*H*), 6.72 (dd, 1H, $J = 16$ Hz, $J = 1.6$ Hz, OHCHC*H*CH), 6.35 (dd, 1H, $J = 16$ Hz, $J = 7.0$ Hz, OHCHCHC*H*), 5.45 (d, 1H, $J = 7.0$ Hz, OHC*H*CHCH) ppm. ^{13}C NMR (101 MHz, $CDCl_3$): δ = 143.63, 136.12, 131.58, 130.89 (q, $J = 32.3$ Hz, *C*CF_3), 130.73, 129.66, 129.03, 128.59, 128.12, 126.75, 124.63–124.57 (m, Ar*C*(H)CCF_3), 124.12 (q, $J = 273.6$ Hz, *C*F_3), 122.93–123.08 (m, Ar*C*(H)CCF_3), 74.63 ppm. ^{19}F NMR (282 MHz, $CDCl_3$) δ = −62.38 ppm. MS(ESI) for $C_{16}H_{13}F_3O$: *m/z* [M]+ calcd 278.09; found 279.20 $[M+H]^+$; FT-IR (KBr) $\nu(cm^{-1})$ = 3457, 3033, 2985, 1664,1751, 1385, 1326, 1154, 1120, 1073, 798, 687.

Synthesis of 3-phenyl-1-(3-(trifluoromethyl)phenyl)propan-1-ol (5c). To a solution of compound (*E*)-3-phenyl-1-(3-(trifluoromethyl)phenyl) prop-2-en-1-one [25] (0.15 g, 0.54 mmol) in MeOH (3.0 mL), $NaBH_4$ (0.020 g, 0.54 mmol) was added and the new mixture was stirred for 1 h at r.t. After the completion of the reaction, the solvent was evaporated, EtOAc was added, and the organic phase was washed with H_2O and brine, dried with Na_2SO_4, filtered, and evaporated. The desired product was obtained after purification by flash column chromatography (silica gel, eluent mixture 9:1, *n*-Hex/EtOAc) and evaporation of the solvent, as oil (95 % yield). Data is consistent with the published literature [46]. ^{1}H NMR (400 MHz, $CDCl_3$): $\delta = 7.63$ (s, 1H, *m*-CF_3-Ph*H*), 7.57–7.53 (m, 2H, *m*-CF_3-Ph*H*), 7.48 (t, 1H, $J = 7.6$ Hz, *m*-CF_3-Ph*H*), 7.30 (t, 2H, $J = 7.4$ Hz, Ph*H*), 7.22–7.18 (m, 3H, Ph*H*), 4.78–4.74 (m, 1H, OHC*H*CH$_2$CH$_2$), 2.80–2.68 (2H, m, OHCHCH$_2$C*H*$_2$), 2.18–2.00 (2H, m, OHCHC*H*$_2$CH$_2$), 1.92 (1H, br. s, OH). ^{13}C NMR (101 MHz, $CDCl_3$) δ = 145.58, 141.31, 131.03 (q, $J = 36.1$ Hz, *C*CF_3), 130.60, 129.24, 128.94, 128.50, 128.42, 126.04, 124.46–124.36 (m, Ar*C*(H)CCF_3), 122.72–122.67 (m, Ar*C*(H)CCF_3), 122.33 (q, $J = 272.8$ Hz, *C*F_3), 73.20, 40.60, 31.92, 29.71 ppm.^{19}F NMR (282 MHz, $CDCl_3$) δ = −62.80 ppm. MS(ESI) for $C_{16}H_{13}F_3O$: *m/z* [M]+ calcd 278.09; found 279.29 $[M+H]^+$. FT-IR (KBr) $\nu(cm^{-1})$ = 3454, 3027, 2970, 1738, 1365, 1326, 1161, 1120, 1071, 803, 698.

Synthesis of N-benzyl-3-(trifluoromethyl)benzamide (9). To a solution of 3-(trifluoromethyl)benzoic acid (0.20 g, 1.1 mmol) in THF (10 mL), HATU (0.44 g, 1.2 mmol) and DIPEA (0.38 mL, 2.2 mmol) were added, and the new solution was stirred for 30 min at r.t. Then, benzylamine (0.13 mL, 1.2 mmol) was added and the new solution was stirred for 3 h at r.t. After the completion of the reaction, the solvent was evaporated, EtOAc was added, and the organic phase was washed with sat. NH_4Cl

and brine, dried with Na_2SO_4, filtered, and evaporated. The desired product was obtained after purification by flash column chromatography (silica gel, eluent mixture 6:4, *n*-Hex/EtOAc) and evaporation of the solvent, as oil (95 % yield). Data is consistent with the published literature [47]. ^{1}H NMR (400 MHz, $CDCl_3$) δ = 8.08 (tt, 1H, *J* = 1.7, 0.7 Hz, *m*-CF_3-Ph*H*), 8.02–7.94 (1H, m, m-CF3-Ph*H*), 7.77 (ddt, 1H, *J* = 7.8, 1.8, 1.0 Hz, *m*-CF_3-Ph*H*), 7.56 (tt, 1H, *J* = 7.8, 0.7 Hz, *m*-CF_3-Ph*H*), 7.43–7.29 (5H, m, Ph*H*), 6.76 (1H, br, s, NH), 4.65 (d, 2H, *J* = 5.7 Hz, CH_2). ^{13}C NMR (101 MHz, $CDCl_3$) δ = 166.02, 137.79, 135.20, 131.63–130.33 (q, *J* = 35.6 Hz, CCF_3), 129.22, 128.85, 128.19–128.08 (m, Ar*C*(H)CCF_3), 127.95, 127.77, 124.00 (q, *J* = 273.0 Hz, CF_3), 124.10–123.98 (m, Ar*C*(H)CCF_3), 44.31 ppm.^{19}F NMR (282 MHz, CDCl3) δ = −62.61 ppm. MS(ESI) for $C_{15}H_{12}F_3NO$: *m/z* [M]+ calcd 279.09; found 280.18 $[M+H]^+$. FT-IR (KBr) $\nu(cm^{-1})$ = 3338, 3069, 3033, 2929, 1642, 1547, 1337, 1276, 1167, 1119, 1074, 922, 824, 726, 695.

Synthesis of N-benzyl-2-(3-(trifluoromethyl)phenyl)acetamide (10). To a solution of 3-(trifluoromethyl)phenylacetic acid (0.20 g, 0.98 mmol) in THF (9.8 mL), HATU (0.41 g, 1.1 mmol) and DIPEA (0.35 mL, 2.0 mmol) were added, and the new solution was stirred for 30 min at r.t. Then, benzylamine (0.12 mL, 1.1 mmol) was added and the new solution was stirred for 3 h at r.t. After the completion of the reaction, the solvent was evaporated, EtOAc was added, and the organic phase was washed with sat. NH_4Cl and brine, dried with Na_2SO_4, filtered, and evaporated. The desired product was obtained after purification by flash column chromatography (silica gel, eluent mixture 1:1, *n*-Hex/EtOAc) and evaporation of the solvent, as oil (75 % yield). ^{1}H NMR (400 MHz, $CDCl_3$) δ = 7.57–7.55 (2H, m, *m*-CF_3-Ph*H*), 7.50–7.44 (2H, m, *m*-CF_3-Ph*H*), 7.35–7.28 (3H, m, Ph*H*), 7.23–7.20 (2H, m, Ph*H*), 6.09 (1H, br. s, NH), 4.41 (2H, s, NHCH_2), 3.62 (2H, s, COCH_2). ^{13}C NMR (101 MHz, CDCl3): δ = 169.96, 137.92, 135.86, 132.76, 131.16 (q, *J* = 33.3 Hz, CCF_3), 129.33, 128.74, 127.63, 127.60, 126.09–125.98 (m, Ar*C*(H)CCF_3), 124.21–124.10 (m, Ar*C*(H)CCF_3), 122.98 (q, *J* = 271.8 Hz, CF_3), 43.77, 43.21 ppm. ^{19}F NMR (282 MHz, CDCl3) δ = −62.61 ppm. MS(ESI) for $C_{16}H_{14}F_3NO$: *m/z* $[M]^+$ calcd 293.10; found 294.94 $[M+H]^+$. FT-IR (KBr) $\nu(cm^{-1})$ = 3282, 3063, 3033, 2930, 2882, 1737, 1644, 1543, 1452, 1331, 1239, 1154, 1114, 1076, 994, 799, 696.

4.2. Biochemical and structural characterization

Reagents 4-aminoantipyrine, 3,5-dichloro-2 hydroxybenzenesulfonic acid, benzylamine, FAD disodium salt hydrate (FAD-Na_2), sodium chloride, HEPES (2-[4-(2-hydroxyethyl)piperazin-1-yl] ethanesulfonic acid) buffer, potassium phosphate, sodium phosphate buffer, glycerol, imidazole, kynuramine, horseradish peroxidase, Safinamide mesylate salt and Triton X-100 were purchased from Sigma-Aldrich. β-octylglucoside (OG), Fos-Choline-12 (Fos-12), Zwittergent 3–12 were purchased from Anatrace (USA).

Expression and purification of human recombinant MAO-B and MAO-A. Human MAO-B and MAO-A were over-expressed in *Pichia pastoris* as described [48]. Human MAO-B was detergent-solubilized using Triton X-100 and purified via Ion Exchange Chromatography (High-Q column, BioRad) following established protocols [48]. Protein concentration was assessed by measuring the flavin absorbance at 456 nm (ε_{456} = 12,000 $M^{-1}cm^{-1}$) with a NanoDrop ND-100 (Thermo Fisher Scientific Inc., MA, USA). Purified protein sample for enzymatic assays was stored in 50 mM potassium phosphate buffer (pH 7.5), 40 % (w/v) glycerol, 0.8 % (w/v) OG. Human MAO-A (His-tagged) was detergent-solubilized using Triton X-100 and purified via Immobilized Metal Affinity Chromatography, as previously reported [48]. Protein concentration was determined using the cofactor spectrum as above. Purified protein sample intended for subsequent enzymatic assays was desalted with a HiTrap® Desalting column (Cytiva) to remove imidazole and stored in 50 mM sodium phosphate buffer (pH 7.8), 300 mM sodium chloride, 40 % (w/v) glycerol, 0.05 % (w/v) Fos-12.

Enzymatic assays. Continuous enzymatic assays were performed following the production of hydrogen peroxide with the spectrophotometric version of the HRP direct coupled assay [49]. Concisely, the reaction was started by adding the enzyme (final concentration, 0.8 μM for MAO-B or MAO-A) to an assay mixture of 50 mM Hepes/NaOH, pH 7.5, 0.25 % (v/v) reduced Triton X-100, 0.1 mM 4-aminoantipyrine, 1 mM 3, 5-dichloro-2 hydroxybenzenesulfonic acid, 13 μg/mL HRP. The absorbance changes were monitored at 515 nm (ε_{515} = 26,000 M^{-1} cm^{-1}) at 25 °C using a spectrophotometer (Cary100; Agilent Technologies, CA, USA). For the initial inhibitor screening, substrates were added at a final concentration of 1.6 mM for benzylamine (MAO-B) and 1.0 mM for kynuramine (MAO-A), and the inhibitors were tested at 20 μM. To determine the inhibition constants (K_i) of MAO-B, assays were conducted by varying benzylamine concentrations in the presence of different concentrations of the inhibitor, following the same experimental procedure as above. Data were fitted to a competitive inhibition model using GraphPad Prism 7.0 software. The experiments were carried out in duplicate, and the K_i values are reported as mean ± SE (standard error) of two independent experiments. Control assays were conducted to evaluate potential interference of the compounds with the peroxidase activity. Briefly, hydrogen peroxide at a concentration of 200 μM was added to the assay mixture in place of MAO-B, while inhibitors were included at a concentration of 20 μM. Minimal to no interference was detected in all experiments.

X-ray crystallography. Human MAO-B was gel filtered in 25 mM potassium phosphate pH 7.5, 8.5 mM Zwittergent 3–12 and co-crystallized with **4a**, **4b**, **4e** and **5a** by the sitting-drop vapour diffusion method following published protocols [25]. Crystals were obtained over about 1 week, then cryo-protected with a mother liquor solution containing 18 % (v/v) glycerol and flash-cooled in liquid nitrogen. X-ray diffraction data were collected at the ID30A-1/MASSIF-1 beamline (for **4b** and **4e** [50], and for **5a** [51]) and at the ID23-2 beamline (**4a,** [52]) (ESRF, Grenoble, France) at 100 K. CCP4 [53] was used for data processing and scaling (Table T1, SI). Coot [54] was used for electron density map inspection and model building. REFMAC5 [55] was used for refinement. Structural data were deposited into the PDB with accession codes 9R2J (**4a**), 9R3K (**4b**), and 9R3J (**4e**). Figures were generated by the program UCSF Chimera X [56].

4.3. In silico analyses

Structure-based calculations. The 7B0V [25] X-ray crystal structure of human MAO-B in complex with SKB was first downloaded from the PDB (https://www.rcsb.org/, last access April 25th, 2025), and then prepared for the *in silico* analyses by using the Protein Preparation Workflow utility of the Schrödinger suite (release 2025-1) [57,58]. Default settings were used during the protein preparation. Afterwards, co-crystallized ions and solvent molecules were removed from the pre-treated structure; waters molecules conserved among the reported MAO-B crystal structures and the FAD cofactor were retained [25,59], and considered as a part of the receptor during the structure-based calculations. Docking calculations were performed on the active site of the prepared receptor by using Glide (Schrödinger suite 2025-1) with default settings [35,36]. The receptor grid was firstly built around the SKB co-crystallized ligand. Then, the ability of the docking protocol to retrieve the correct binding mode of SKB was tested by redocking it into the prepared 7B0V receptor. Then, the investigated compounds (see Table 1) were prepared for docking by using LigPrep (default settings) [36]; tautomers and protonation states potentially present at physiological pH were generated, and stereoisomers sampling was performed for ligands with undefined stereochemistry centers. Afterwards, the prepared compounds were docked into the MAO-B receptor. A visual inspection of the predicted poses, in combination with results of Prime MM-GBSA calculations (Schrödinger suite 2025-1) [36] conducted with default settings, aided in the definition of the structure-activity relationships of the compounds.

Analyses of selected molecular descriptors. The drug-likeness and

Table 3
Selected ADME-related molecular descriptors of the compounds investigated in this study.

Compound	QPPCaco	QPlogKhsa	QPlogPo/w	QPlogS	Glob	NumHBA	NumHBD
1	3711.9	0.5	4.6	−5.1	0.8	1	0
4a	442.2	0.4	3.8	−5.1	0.8	3	0
4b	442.5	0.4	3.8	−5.1	0.8	3	0
4c	4461.5	0.6	5.2	−5.7	0.8	1	0
4d	3720.9	0.8	5.6	−6.6	0.8	1	0
4e	3712.2	0.2	4.0	−4.3	0.9	3	0
4f	1088.4	−0.1	2.7	−3.8	0.9	2	1
4g	1312.9	0.01	2.9	−3.9	0.9	2	1
5a	3975.5	0.5	4.8	−5.2	0.8	1	0
5b	3625.3	0.5	4.9	−4.9	0.8	1	1
5c	4339.9	0.6	4.8	−5.0	0.8	1	1
9	4004.9	0.4	4.6	−4.9	0.8	1	1
10	3168.8	0.2	4.1	−4.8	0.8	1	1

Values outside recommended ranges QikProp are highlighted in red. Recommended value ranges according to the QikProp (Schrödinger 2025-1) manual are the following: **QPPCaco** (predicted apparent Caco-2 cell permeability in nm/sec.): <25 poor, >500 great; **QplogKhsa** (estimated binding to human serum albumin): 1.5 – 1.5; **QPlogPo/w** (predicted octanol/water partition coefficient): 2.0 – 6.5; **QplogS** (predicted aqueous solubility): 6.5 – 0.5; **Glob** (predicted globularity): 0.75–0.95; **NumHBA** (estimated number of hydrogen bonds that would be accepted by the compound): 0–20; **NumHBD** (estimated number of hydrogen bonds that would be donated by the compound): 0–6 (Ghose's recommended range: <3).

potential blood-brain-barrier permeability of the compounds investigated in this study were *in silico* investigated. To this end, the chalcone-based inhibitors previously prepared for the docking calculations with LigPrep [36] (vide supra) were subjected to ADME predictions using QikProp (Schrödinger suite 2025-1) [39]. Moreover, TPSA of the prepared compounds was calculated by means of a python script based on the RDKit libraries (https://www.rdkit.org/, accessed on 11 July 2025). Default parameters were employed for the molecular descriptors calculation. This analysis enabled the evaluation of selected physico-chemical and pharmacokinetic descriptors to be compared with commonly accepted drug-likeness ranges. A detailed summary of the calculated properties for the compounds is provided in Tables 2 and 3.

4.4. Cell viability and neuroprotection studies

Drugs. Rates of anti-MAO new molecules: **4a**, **4e** and **5a** were prepared at the concentration of 10 mg/mL (stock solution) in dimethyl sulfoxide (DMSO, Sigma-Aldrich, USA). 6-OHDA was prepared at the concentration of 200 μg/mL in complete culture medium. Working solutions were freshly prepared according to the experimental design by serial dilutions in complete culture medium.

Cell lines. The *in vitro* activity of the molecules was tested against human dermal fibroblasts (hSDFs) [60] adipose tissue derived mesenchymal stromal cells (AT -MSCs) [61], and also on human cancer cells (human melanoma A-375 [62]; glioblastoma U87-MG [63], and neuroblastoma SH-SY5Y [64]. The cells were maintained by 1:10, 1:20 weekly dilution in Eagle's minimum essential (EMEM) medium (hSDFs) and DMEM LG medium supplemented with 10 % FBS (fetal bovine serum) and 2 mM L-glutamine and incubated at 37 °C, 5 % CO_2. All reagents for cell cultures were provided by Euroclone (Pero MI, Italy).

In vitro antiproliferation assay on normal and cancer cells. The cell viability in response to compound treatment was evaluated in 96 multiwell plates (Euroclone, Pero MI, Italy). Briefly, the biocompatibility of compounds **4a**, **4e** and **5a** (tested at concentrations from 0.31 to 40 μM) was assessed by adding 2×10^3 cells in 100 μl of culture medium containing the respective compound in each well. After 7 days (anti-proliferative assay) at 37 °C, 5 % CO_2, cell viability was evaluated by MTT assay (3-(4,5-dimethyl-2-thiazolyl)-2,5-diphenyl-2-H-tetrazolium) as previously described [65,66].

In vitro cytotoxicity and neuroprotection evaluation on neuroblastoma cells. The cell viability in response to treatment with **5a** or with 6-OHDA was evaluated with MTT assay after 2 h at different concentrations (from 0.78 to 100 μM) and expressed as the percentage of viable cells compared to untreated cells (control). The evaluation of the neuroprotective effect of **5a** was performed by pre-treating 10×10^3 SH-SY5Y cells with the compound for 2 h (concentrations of 12.5-25-50 and 100 μM) at 37 °C, 5 % CO_2 and after the following 24 h incubation with 6-OHDA at increasing concentrations from 62.5 μM to 250 μM. The inhibitory concentrations (IC_{50}) were determined according to the linearity regression or Reed & Muench formula [67] by using Excel (Microsoft, Inc, Albuquerque, NM, USA).

Statistical Analysis. Data were expressed as mean ± standard deviation (SD). Differences between mean values were evaluated using Analysis of Variance (ANOVA) with a Student-Newman-Keuls Multiple Comparisons Test and Dunnett Multiple Comparisons Test performed by the GRAPHPADINSTAT program (GraphPad Software Inc., San Diego, CA, USA). The p-values ≤0.05 were considered statistically significant. The linearity of response and correlation were analyzed using regression analysis with Excel 2013 software (Microsoft, Inc., Albuquerque, New Mexico, USA).

CRediT authorship contribution statement

Giorgio Facchetti: Writing – review & editing, Writing – original draft, Methodology, Investigation, Formal analysis, Data curation. **Sara Marchese:** Writing – review & editing, Writing – original draft, Methodology, Investigation, Formal analysis. **Valentina Coccè:** Writing – review & editing, Investigation, Data curation. **Luisa Doneda:** Writing – review & editing, Data curation. **Giulio Alessandri:** Writing – review & editing, Data curation. **Francesca Paino:** Writing – review & editing, Data curation. **Augusto Pessina:** Writing – review & editing, Writing – original draft, Validation, Methodology, Formal analysis. **Luca Pinzi:** Writing – review & editing, Writing – original draft, Formal analysis, Data curation. **Giulio Rastelli:** Writing – review & editing, Methodology. **Claudia Binda:** Writing – review & editing, Validation, Supervision, Resources, Project administration, Methodology, Funding acquisition, Formal analysis, Conceptualization. **Michael S. Christodoulou:** Writing – review & editing, Writing – original draft, Validation, Supervision, Resources, Project administration, Methodology, Investigation, Funding acquisition, Formal analysis, Data curation, Conceptualization. **Isabella Rimoldi:** Writing – review & editing, Writing – original draft, Validation, Supervision, Resources, Project administration, Methodology, Funding acquisition, Formal analysis, Conceptualization.

Accession codes

The coordinates and structure factors have been deposited in the PDB under accession codes 9R2J (**4a**), 9R3K (**4b**), and 9R3J (**4e**).

Funding sources

This was supported by MUR - P.R.I.N. 2022 (D.D. n. 104 del 02-02-2022) with the grant n. 2022LWZ77 N_001 (to CB).

Declaration of competing interest

The authors declare the following financial interests/personal relationships which may be considered as potential competing interests: Isabella Rimoldi reports financial support provided by University of Milan. Isabella Rimoldi reports a relationship with University of Milan that includes: board membership. Nothing to declare If there are other authors, they declare that they have no known competing financial interests or personal relationships that could have appeared to influence the work reported in this paper.

Acknowledgments

We acknowledge ESRF and EMBL Grenoble for assistance and support in using X-ray beamlines ID30A-1/MASSIF-1 and ID23-2 under proposal number MX-2503 and MX-2591.

Appendix A. Supplementary data

Supplementary data to this article can be found online at https://doi.org/10.1016/j.ejmech.2025.117990.

Data availability

Data will be made available on request.

References

[1] Z. Rozmer, P. Perjési, Naturally occurring chalcones and their biological activities, Phytochem. Rev. 15 (2016) 87–120.
[2] G. Di Carlo, N. Mascolo, A.A. Izzo, F. Capasso, Flavonoids: old and new aspects of a class of natural therapeutic drugs, Life Sci. 65 (1999) 337–353.
[3] C. Zhuang, W. Zhang, C. Sheng, W. Zhang, C. Xing, Z. Miao, Chalcone: a privileged structure in medicinal chemistry, Chem. Rev. 117 (2017) 7762–7810.
[4] R. Gandolfi, G. Facchetti, M.S. Christodoulou, M. Fusè, F. Meneghetti, I. Rimoldi, Cascade reaction by chemo- and biocatalytic approaches to obtain chiral hydroxy ketones and anti 1,3-Diols, Chemist 7 (2018) 393–400.
[5] D. Elkhalifa, I. Al-Hashimi, A.E. Al Moustafa, A. Khalil, A comprehensive review on the antiviral activities of chalcones, J. Drug Target. 29 (2021) 403–419.
[6] A. Mittal, V.K. Vashistha, D.K. Das, Recent advances in the antioxidant activity and mechanisms of chalcone derivatives: a computational review, Free Radic. Res. 56 (2022) 378–397.
[7] B. Salehi, C. Quispe, I. Chamkhi, N. El Omari, A. Balahbib, J. Sharifi-Rad, A. Bouyahya, M. Akram, M. Iqbal, A.O. Docea, C. Caruntu, G. Leyva-Gómez, A. Dey, M. Martorell, D. Calina, V. López, F. Les, Pharmacological properties of chalcones: a review of preclinical including molecular mechanisms and clinical evidence, Front. Pharmacol. 11 (2021), 2020.
[8] B. Salehi, C. Quispe, I. Chamkhi, N. El Omari, A. Balahbib, J. Sharifi-Rad, A. Bouyahya, M. Akram, M. Iqbal, A.O. Docea, C. Caruntu, G. Leyva-Gómez, A. Dey, M. Martorell, D. Calina, V. López, F. Les, Pharmacological properties of chalcones: a review of preclinical including molecular mechanisms and clinical evidence, Front. Pharmacol. 11 (2020) 592654.
[9] A. Moriello, L. Luongo, F. Guida, M. Christodoulou, D. Perdicchia, S. Maione, D. Passarella, V. Di Marzo, L. De petrocellis, Chalcone derivatives activate and desensitize the transient receptor potential ankyrin 1 cation channel, subfamily A, member 1 TRPA1 ion channel: structure-activity relationships in vitro and anti-nociceptive and anti-inflammatory activity in vivo, CNS Neurol. Disord.: Drug Targets 15 (2016).
[10] M.D. Canela, S. Noppen, O. Bueno, A.E. Prota, K. Bargsten, G. Sáez-Calvo, M. L. Jimeno, M. Benkheil, D. Ribatti, S. Velázquez, M.J. Camarasa, J.F. Díaz, M. O. Steinmetz, E.M. Priego, M.J. Pérez-Pérez, S. Liekens, Antivascular and antitumor properties of the tubulin-binding chalcone TUB091, Oncotarget 8 (2017) 14325–14342.
[11] I.D. Sahin, M.S. Christodoulou, E.A. Guzelcan, A. Koyas, C. Karaca, D. Passarella, R. Cetin-Atalay, A small library of chalcones induce liver cancer cell death through Akt phosphorylation inhibition, Sci. Rep. 10 (2020) 11814.
[12] E. Corsini, G. Facchetti, S. Esposito, A. Maddalon, I. Rimoldi, M.S. Christodoulou, Antiproliferative effects of chalcones on T cell acute lymphoblastic leukemia-derived cells: role of PKCβ, Arch. Pharm. (2020) e2000062, 2000010.2001002/ardp.202000062.
[13] D. Quaglio, N. Zhdanovskaya, G. Tobajas, V. Cuartas, S. Balducci, M. S. Christodoulou, G. Fabrizi, M. Gargantilla, E.-M. Priego, Á. Carmona Pestaña, D. Passarella, I. Screpanti, B. Botta, R. Palermo, M. Mori, F. Ghirga, M.-J. Pérez-Pérez, Chalcones and chalcone-mimetic derivatives as notch inhibitors in a model of T-cell acute lymphoblastic leukemia, ACS Med. Chem. Lett. 10 (2019) 639–643.
[14] E. Merve Aydin, İ.S. Canıtez, E. Colombo, S. Princiotto, D. Passarella, S. Dallavalle, M.S. Christodoulou, I. Durmaz Şahin, Targeting ovarian cancer with chalcone derivatives: cytotoxicity and apoptosis induction in HGSOC cells, Molecules 28 (2023) 7777.
[15] F. Chimenti, R. Fioravanti, A. Bolasco, P. Chimenti, D. Secci, F. Rossi, M. Yáñez, F. Orallo, F. Ortuso, S. Alcaro, Chalcones: a valid scaffold for monoamine oxidases inhibitors, J. Med. Chem. 52 (2009) 2818–2824.
[16] F. Melfi, S. Carradori, A. Angeli, I. D'Agostino, Nature as a source and inspiration for human monoamine oxidase B (hMAO-B) inhibition: a review of the recent advances in chemical modification of natural compounds, Expet Opin. Drug Discov. 18 (2023).
[17] B. Mathew, Unraveling the structural requirements of chalcone chemistry towards monoamine oxidase inhibition, Cent. Nerv. Syst. Agents Med. Chem. 19 (2019) 6–7.
[18] B. Mathew, A. Haridas, J. Suresh, G.E. Mathew, G. Uçar, V. Jayaprakash, Monoamine oxidase inhibitory action of chalcones: a mini review, Cent. Nerv. Syst. Agents Med. Chem. 16 (2016) 120–136.
[19] R. Shalaby, J.P. Petzer, A. Petzer, U.M. Ashraf, E. Atari, F. Alasmari, S. Kumarasamy, Y. Sari, A. Khalil, SAR and molecular mechanism studies of monoamine oxidase inhibition by selected chalcone analogs, J. Enzym. Inhib. Med. Chem. 34 (2019) 863–876.
[20] J. Harris, E. Boekema, Membrane Protein Complexes: Structure and Function, 2018.
[21] R.M. Geha, I. Rebrin, K. Chen, J.C. Shih, Substrate and inhibitor specificities for human monoamine oxidase A and B are influenced by a single amino acid, J. Biol. Chem. 276 (2001) 9877–9882.
[22] M.B. Youdim, D. Edmondson, K.F. Tipton, The therapeutic potential of monoamine oxidase inhibitors, Nat. Rev. Neurosci. 7 (2006) 295–309.
[23] R.K.P. Tripathi, S.R. Ayyannan, Monoamine oxidase-B inhibitors as potential neurotherapeutic agents: an overview and update, Med. Res. Rev. 39 (2019) 1603–1706.
[24] M. Paolo, M. Christodoulou, A. Calogero, L. Pinzi, G. Rastelli, D. Passarella, G. Cappelletti, L. Dalla Via, 2-Phenyloxazole-4-carboxamide as a scaffold for selective inhibition of human monoamine oxidase B, ChemMedChem 14 (2019).
[25] L.G. Iacovino, L. Pinzi, G. Facchetti, B. Bortolini, M.S. Christodoulou, C. Binda, G. Rastelli, I. Rimoldi, D. Passarella, M.L. Di Paolo, L. Dalla Via, Promising non-cytotoxic monosubstituted chalcones to target monoamine Oxidase-B, ACS Med. Chem. Lett. (2021) 1151–1158.
[26] C. Binda, J. Wang, L. Pisani, C. Caccia, A. Carotti, P. Salvati, D.E. Edmondson, A. Mattevi, Structures of human monoamine oxidase B complexes with selective noncovalent inhibitors: safinamide and coumarin analogs, J. Med. Chem. 50 (2007) 5848–5852.
[27] C. Binda, D.E. Edmondson, A. Mattevi, Crystallization of human monoamine oxidase B, Methods Mol. Biol. 2558 (2023) 115–122.
[28] S. Cetin, D. Knez, S. Gobec, J. Kos, A. Pišlar, Cell models for Alzheimer's and Parkinson's disease: at the interface of biology and drug discovery, Biomed. Pharmacother. 149 (2022) 112924.
[29] R. Gandolfi, G. Facchetti, L. Cavalca, S. Mazzini, M. Colombo, G. Coffetti, G. Borgonovo, L. Scaglioni, S. Zecchin, I. Rimoldi, Hybrid catalysts from copper biosorbing bacterial strains and their recycling for catalytic application in the asymmetric addition reaction of B2(pin)2 on α,β-Unsaturated chalcones, Catalysts 12 (2022) 433.
[30] S.F. Nielsen, A. Kharazmi, S.B. Christensen, Modifications of the alpha,beta-double bond in chalcones only marginally affect the antiprotozoal activities, Bioorg. Med. Chem. 6 (1998) 937–945.
[31] J.L. Luche, Lanthanides in organic chemistry. 1. Selective 1,2 reductions of conjugated ketones, J. Am. Chem. Soc. 100 (1978) 2226–2227.
[32] J.-L. Luche, L. Rodriguez-Hahn, P. Crabbé, Reduction of natural enones in the presence of cerium trichloride, Chem. Commun. (1978) 601–602.
[33] D.E. Edmondson, C. Binda, J. Wang, A.K. Upadhyay, A. Mattevi, Molecular and mechanistic properties of the membrane-bound mitochondrial monoamine oxidases, Biochemistry 48 (2009) 4220–4230.
[34] J. Reis, N. Manzella, F. Cagide, J. Mialet-Perez, E. Uriarte, A. Parini, F. Borges, C. Binda, Tight-binding inhibition of human monoamine oxidase B by chromone analogs: a kinetic, crystallographic, and biological analysis, J. Med. Chem. 61 (2018) 4203–4212.
[35] R.A. Friesner, J.L. Banks, R.B. Murphy, T.A. Halgren, J.J. Klicic, D.T. Mainz, M. P. Repasky, E.H. Knoll, M. Shelley, J.K. Perry, D.E. Shaw, P. Francis, P.S. Shenkin, Glide: a new approach for rapid, accurate docking and scoring. 1. Method and assessment of docking accuracy, J. Med. Chem. 47 (2004) 1739–1749.
[36] S. Schrödinger Release 2025-1: Glide, LLC, New York, NY, 2025.
[37] B. Mathew, S.C. Baek, D.G. Thomas Parambi, J.P. Lee, G.E. Mathew, S. Jayanthi, D. Vinod, C. Rapheal, V. Devikrishna, S.S. Kondarath, M.S. Uddin, H. Kim, Potent and highly selective dual-targeting monoamine oxidase-B inhibitors: fluorinated chalcones of morpholine versus imidazole, Arch. Pharm. 352 (2019) 1800309.
[38] S.T. Sudevan, J.M. Oh, M.A. Abdelgawad, M.A.S. Abourehab, T.M. Rangarajan, S. Kumar, I. Ahmad, H. Patel, H. Kim, B. Mathew, Introduction of benzyloxy pharmacophore into aryl/heteroaryl chalcone motifs as a new class of monoamine oxidase B inhibitors, Sci. Rep. 12 (2022) 22404.
[39] Schrödinger Release 2025-1: Qikprop, Schrödinger, LLC, New York, NY, 2025.

[40] A.K. Ghose, T. Herbertz, R.L. Hudkins, B.D. Dorsey, J.P. Mallamo, Knowledge-based, Central Nervous System (CNS) lead selection and lead optimization for CNS drug discovery, ACS Chem. Neurosci. 3 (2012) 50–68.
[41] Y. Fan, J. Wang, J. Jian, Y. Wen, J. Li, H. Tian, J. Crommen, W. Bi, T. Zhang, Z. Jiang, High-throughput discovery of highly selective reversible hMAO-B inhibitors based on at-line nanofractionation, Acta Pharm. Sin. B 14 (2024) 1772–1786.
[42] S. Chakrabarti, M. Bisaglia, Oxidative stress and neuroinflammation in Parkinson's disease: the role of dopamine oxidation products, Antioxidants 12 (2023).
[43] C.J. Thomson, D.M. Barber, D.J. Dixon, One-pot catalytic enantioselective synthesis of 2-Pyrazolines, Angew. Chem. Int. Ed. 58 (2019) 2469–2473.
[44] X.-B. Lan, Z. Ye, J. Liu, M. Huang, Y. Shao, X. Cai, Y. Liu, Z. Ke, Sustainable and selective alkylation of deactivated secondary alcohols to ketones by non-bifunctional pincer N-heterocyclic carbene manganese, ChemSusChem 13 (2020) 2557–2563.
[45] J. Ma, W. Li, L. He, H. Lv, Iridium-catalyzed chemoselective asymmetric hydrogenation of conjugated enones with ferrocene-based multidentate phosphine ligands, Chem. Commun. 58 (2022) 5841–5844.
[46] T. Liu, L. Wang, K. Wu, Z. Yu, Manganese-catalyzed β-Alkylation of secondary alcohols with primary alcohols under phosphine-free conditions, ACS Catal. 8 (2018) 7201–7207.
[47] F. Li, P. Qu, J. Ma, X. Zou, C. Sun, Tandem synthesis of N-Alkylated amides from aldoximes and alcohols by using a Ru/Ir dual-catalyst system, ChemCatChem 5 (2013) 2178–2182.
[48] D.E. Edmondson, Purification of recombinant eukaryotic MAO A and MAO B utilizing the Pichia pastoris expression system, Methods Mol. Biol. 2558 (2023) 11–22.
[49] J. Reis, C. Binda, The peroxidase-coupled assay to measure MAO enzymatic activity, Methods Mol. Biol. 2558 (2023) 23–34.
[50] M. Barone, L. Basile, D. Carraretto, D. Cecchini, M. Malatesta, S. Marchese, G. Tjallinks, Proteins related to pathogenesis of diseases, viral proteins, cell division, signalling and chromatin processes, European Synchrotron Radiation Facility (2025). https://doi.org/10.15151/ESRF-ES-1716079795.
[51] D. Cecchini, A. Gottinger, S. Marchese, Proteins related to pathogenesis of diseases, viral proteins, cell division, signalling and chromatin processes, European Synchrotron Radiation Facility (2025). https://doi.org/10.15151/ESRF-ES-1934156944.
[52] L. Basile, A. Canciani Anselmo, D. Carraretto, F. Forneris, B. Guerriere, S. Marchese, C.R. Nicoll, Proteins related to pathogenesis of diseases, viral proteins, cell division, signalling and chromatin processes, European Synchrotron Radiation Facility (2025). https://doi.org/10.15151/ESRF-ES-1059290596.
[53] J. Agirre, M. Atanasova, H. Bagdonas, C.B. Ballard, A. Baslé, J. Beilsten-Edmands, R.J. Borges, D.G. Brown, J.J. Burgos-Mármol, J.M. Berrisford, P.S. Bond, I. Caballero, L. Catapano, G. Chojnowski, A.G. Cook, K.D. Cowtan, T.I. Croll, J. Debreczeni, N.E. Devenish, E.J. Dodson, T.R. Drevon, P. Emsley, G. Evans, P. R. Evans, M. Fando, J. Foadi, L. Fuentes-Montero, E.F. Garman, M. Gerstel, R. J. Gildea, K. Hatti, M.L. Hekkelman, P. Heuser, S.W. Hoh, M.A. Hough, H. T. Jenkins, E. Jiménez, R.P. Joosten, R.M. Keegan, N. Keep, E.B. Krissinel, P. Kolenko, O. Kovalevskiy, V.S. Lamzin, D.M. Lawson, A.A. Lebedev, A.G. W. Leslie, B. Lohkamp, F. Long, M. Malý, A.J. McCoy, S.J. McNicholas, A. Medina, C. Millán, J.W. Murray, G.N. Murshudov, R.A. Nicholls, M.E.M. Noble, R. Oeffner, N.S. Pannu, J.M. Parkhurst, N. Pearce, J. Pereira, A. Perrakis, H.R. Powell, R. J. Read, D.J. Rigden, W. Rochira, M. Sammito, F. Sánchez Rodríguez, G. M. Sheldrick, K.L. Shelley, F. Simkovic, A.J. Simpkin, P. Skubak, E. Sobolev, R. A. Steiner, K. Stevenson, I. Tews, J.M.H. Thomas, A. Thorn, J.T. Valls, V. Uski, I. Usón, A. Vagin, S. Velankar, M. Vollmar, H. Walden, D. Waterman, K.S. Wilson, M.D. Winn, G. Winter, M. Wojdyr, K. Yamashita, The CCP4 suite: integrative software for macromolecular crystallography, Acta Crystallogr D Struct Biol 79 (2023) 449–461.
[54] P. Emsley, B. Lohkamp, W.G. Scott, K. Cowtan, Features and development of coot, Acta Crystallogr D Biol Crystallogr 66 (2010) 486–501.
[55] O. Kovalevskiy, R.A. Nicholls, F. Long, A. Carlon, G.N. Murshudov, Overview of refinement procedures within REFMAC5: utilizing data from different sources, Acta Crystallogr D Struct Biol 74 (2018) 215–227.
[56] E.C. Meng, T.D. Goddard, E.F. Pettersen, G.S. Couch, Z.J. Pearson, J.H. Morris, T. E. Ferrin, UCSF ChimeraX: tools for structure building and analysis, Protein Sci. 32 (2023) e4792.
[57] G. Madhavi Sastry, M. Adzhigirey, T. Day, R. Annabhimoju, W. Sherman, Protein and ligand preparation: parameters, protocols, and influence on virtual screening enrichments, J. Comput. Aided Mol. Des. 27 (2013) 221–234.
[58] S. Schrödinger, Release 2025-1: Protein Preparation Workflow; Epik, LLC, New York, NY, 2024; Impact, Schrödinger, LLC, Schrödinger, LLC, New York, NY; Prime, 2025. New York, NY.
[59] S. Distinto, M. Yáñez, S. Alcaro, M.C. Cardia, M. Gaspari, M.L. Sanna, R. Meleddu, F. Ortuso, J. Kirchmair, P. Markt, A. Bolasco, G. Wolber, D. Secci, E. Maccioni, Synthesis and biological assessment of novel 2-thiazolylhydrazones and computational analysis of their recognition by monoamine oxidase B, Eur. J. Med. Chem. 48 (2012) 284–295.
[60] V. Coccè, A. Vitale, S. Colombo, A. Bonomi, F. Sisto, E. Ciusani, G. Alessandri, E. Parati, P. Brambilla, M. Brambilla, C.A. La Porta, A. Pessina, Human skin-derived fibroblasts used as a 'Trojan horse' for drug delivery, Clin. Exp. Dermatol. 41 (2016) 417–424.
[61] A. Bonomi, V. Coccè, L. Cavicchini, F. Sisto, M. Dossena, N. Balzarini, Adipose tissue-derived stromal cells primed in vitro with paclitaxel acquire anti-tumor activity, Int. J. Immunopathol. Pharmacol. 26 (2013).
[62] D.J. Giard, S.A. Aaronson, G.J. Todaro, P. Arnstein, J.H. Kersey, H. Dosik, W. P. Parks, In vitro cultivation of human tumors: establishment of cell lines derived from a series of solid tumors, J. Natl. Cancer Inst. 51 (1973) 1417–1423.
[63] J. Fogh, J.M. Fogh, T. Orfeo, One hundred and twenty-seven cultured human tumor cell lines producing tumors in nude mice, J Natl Cancer Inst 59 (1977) 221–226.
[64] R.A. Ross, B.A. Spengler, J.L. Biedler, Coordinate morphological and biochemical interconversion of human neuroblastoma cells, J. Natl. Cancer Inst. 71 (1983) 741–747.
[65] A. Pessina, L. Gribaldo, E. Mineo, M.G. Neri, In vitro short-term and long-term cytotoxicity of fluoroquinolones on murine cell lines, Indian J. Exp. Biol. 32 (1994) 113–118.
[66] T. Mosmann, Rapid colorimetric assay for cellular growth and survival: application to proliferation and cytotoxicity assays, J. Immunol. Methods 65 (1983) 55–63.
[67] H. Muench Reed, A simple method of estimating fifty per cent endpoints, Am. J. Epidemiol. 27 (1938) 493–497.